

# Noise-Assisted Metastability: From Lévy Flights to Memristors, Quantum Escape, and Josephson-based Axion Searches

Quantum Economics and Finance  
XX(X):1–23  
©The Author(s) 2026  
Reprints and permission:  
[sagepub.co.uk/journalsPermissions.nav](http://sagepub.co.uk/journalsPermissions.nav)  
DOI: 10.1177/ToBeAssigned  
[www.sagepub.com/](http://www.sagepub.com/)



Claudio Guarcello<sup>1,2</sup>, Alexander A. Dubkov<sup>3</sup>, Davide Valenti<sup>4</sup>, Bernardo Spagnolo<sup>4,5</sup>

## Abstract

Many-body and complex systems, both classical and quantum, often exhibit slow, nonlinear relaxation toward stationary states due to the presence of metastable configurations and environmental fluctuations. Nonlinear relaxation in a wide variety of natural systems proceeds through metastable states, which arise in condensed-matter physics as well as in fields ranging from cosmology and biology to high-energy physics. Moreover, noise-induced phenomena play a central role in shaping the dynamics of such systems far from equilibrium. This review develops a unifying perspective centered on noise-assisted stabilization and the statistical properties of metastable dynamics. We first discuss escape processes driven by Lévy flights in smooth metastable potentials, emphasizing the emergence of nonmonotonic residence-time behavior. We then connect these concepts to stochastic resistive switching in memristive devices, where noise-induced effects can enhance stability and reproducibility. We further examine driven dissipative quantum bistability, showing how the interplay between external driving and system–environment coupling reshapes escape pathways and lifetimes. Finally, we outline how switching-time statistics in current-biased Josephson junctions can provide an experimentally accessible strategy for axion detection, based on an axion-induced resonant-activation signature.

## Keywords

metastability, noise-enhanced stability, Lévy noise, switching-time statistics, stochastic resonance, resonant activation

## 1 Introduction

In this paper, we briefly review recent results that collectively elucidate the nontrivial role of noise, dissipation, and external driving in stabilizing and controlling metastable states in both quantum and classical systems. We emphasize the constructive role of noise in the dynamics of complex systems and highlight a unifying theme: the counterintuitive enhancement of stability induced by fluctuations, which challenges the traditional view of noise as purely detrimental.

Metastable states are a characteristic feature of nonlinear complex systems and govern relaxation, switching, and escape phenomena in physics, chemistry, and materials science. The effects of Gaussian noise on metastability are well understood, most notably through Kramers' theory and its generalizations to nonlinear potentials and nonequilibrium initial conditions (Agudov et al. 2003). However, many physical systems are instead subject to non-Gaussian fluctuations characterized by rare but large events. Such fluctuations are naturally described by Lévy

noise, which exhibits heavy-tailed statistics and formally infinite variance. The work reported by Dubkov et al. (2025) addresses the fundamental question of how Lévy noise affects the stability of metastable states. Remarkably, Lévy noise enhances metastable stability and gives rise to asymptotic behavior in the zero-noise limit that is

<sup>1</sup>Dipartimento di Fisica “E. R. Caianiello”, Università degli Studi di Salerno, I-84084 Fisciano, Salerno, Italy <sup>2</sup>INFN, Sezione di Napoli, Gruppo Collegato di Salerno – Complesso Universitario di Monte S. Angelo, I-80126 Napoli, Italy <sup>3</sup>Radiophysics Department, Lobachevsky State University, 603950 Nizhniy Novgorod, Russia <sup>4</sup>Dipartimento di Fisica e Chimica “E. Segrè”, Group of Interdisciplinary Theoretical Physics, Università degli Studi di Palermo, I-90128 Palermo, Italy <sup>5</sup>Stochastic Multistable Systems Laboratory, Lobachevsky University, 603950 Nizhniy Novgorod, Russia

## Corresponding author:

Bernardo Spagnolo, Dipartimento di Fisica e Chimica “E. Segrè”, Group of Interdisciplinary Theoretical Physics, Università degli Studi di Palermo, I-90128 Palermo, Italy.

Email: [bernardo.spagnolo@unipa.it](mailto:bernardo.spagnolo@unipa.it)

fundamentally different from the Gaussian case. This finding generalizes the concept of noise-enhanced stability to non-Gaussian stochastic dynamics. In particular, exact results have been obtained for the mean residence time (MRT) of a particle moving in an arbitrary smooth potential with a sink under Lévy noise with arbitrary Lévy index  $\alpha$  and noise intensity. Moreover, a closed expression in quadrature for the MRT has been derived for Lévy flights with  $\alpha = 1$  (Cauchy noise) in a cubic metastable potential, analytically demonstrating the enhancement of metastable stability induced by Lévy noise (Dubkov et al. 2025). These results broaden the theoretical framework and underscore the universality of noise-assisted stabilization phenomena.

The constructive role of noise is not only of theoretical relevance but also emerges clearly in solid-state devices. Memristors, for example, are multistable systems whose switching dynamics is intrinsically stochastic, as consistently observed in experiments. To employ memristors as functional elements in resistive random access memory (RRAM) and neuromorphic architectures, it is essential to deepen our understanding of the resistive state switching process, accounting for multistability, internal and external noise sources, and metastable states in the transient nonlinear dynamics of these nonequilibrium systems. In Agudov et al. (2020), Filatov et al. (2022) and Koryazhina et al. (2022), the first experimental evidence of noise-enhanced stability in  $\text{ZrO}_2(\text{Y})$  memristors was reported. A stochastic model introduced by Agudov et al. (2020) predicts a nonmonotonic dependence of the relaxation time on fluctuation intensity, in good agreement with experimental observations (Koryazhina et al. 2022). These works demonstrate that noise can either slow down or accelerate switching depending on its nature and strength, and that noise can play a genuinely constructive role in memristive systems. Furthermore, another paradigmatic noise-induced phenomenon—stochastic resonance—has been experimentally observed in metal-oxide memristive devices (Mikhaylov et al. 2021).

Metastability and noise-assisted phenomena are equally central in quantum systems. Metastable states appear in a wide range of quantum platforms, from superconducting circuits and cold atoms to chemical reactions and condensed-matter systems. Traditionally, dissipation and noise have been regarded as mechanisms that accelerate decay and destroy quantum coherence. However, growing evidence indicates that dissipation and quantum fluctuations, when properly engineered, can instead be exploited as a resource to control quantum dynamics. Valenti et al. (2018) explores this paradigm shift by analyzing how external driving and dissipation can stabilize quantum metastable states rather than acting solely as sources of decoherence. The study demonstrates that the interplay

between coherent driving, dissipation, and quantum fluctuations can significantly prolong the lifetime of metastable states, revealing a genuine quantum analogue of the noise-enhanced stability observed in classical systems (Agudov et al. 2003). Specifically, it is shown that increasing the system–environment coupling drives a transition in the escape dynamics: from a regime where the escape time is strongly controlled by the external driving and exhibits resonant peaks and dips, to a regime where the escape time becomes frequency independent, characterized by a single peak followed by a steep decrease. The escape time displays a nonmonotonic dependence on bath coupling, temperature, and driving frequency, providing clear evidence of quantum noise-enhanced stability and quantum resonant activation in the investigated system.

Finally, these concepts also open new perspectives in fundamental physics and sensing technologies. The search for axions and axion-like particles as viable dark matter candidates remains one of the most compelling challenges in modern physics. Conventional detection strategies—such as those exploiting the Primakoff effect in microwave cavities—rely on the conversion of axions into photons in strong magnetic fields, but suffer from limitations in sensitivity and broadband coverage over wide axion mass ranges. In this context, superconducting devices, and in particular Josephson junctions (JJs), have emerged as promising alternatives owing to their intrinsic sensitivity to weak perturbations and their tunable dynamical properties (Grimaudo et al. 2022). The phenomenon of resonant activation in a current-biased Josephson junction was proposed by Grimaudo et al. (2022) as a mechanism for axion detection. The key conceptual advance lies in coupling the axion field to the JJ dynamics such that the effective escape dynamics of the phase particle in the tilted washboard potential are modified by the presence of the axion field. This coupling manifests as a nonmonotonic dependence of the mean switching time—from the superconducting to the resistive state—on the ratio between the axion energy and the Josephson plasma energy. When this ratio approaches unity, a resonant condition enhances the switching probability, providing a distinct axion-induced signature in the switching-time statistics that could be exploited experimentally.

## 2 Lévy-noise-induced enhancement of stabilization of metastable states

In this section, we discuss escape from metastability under symmetric  $\alpha$ -stable Lévy noise, emphasizing the noise-enhanced stability scenario that emerges when analyzing the mean residence time in a prescribed interval. We summarize the role of boundary conditions and geometric parameters defining the observation window. The resulting

parameter dependence provides a compact characterization of Lévy-induced stabilization effects and of their signatures in trajectory data.

Escape from a metastable state is a standard framework for noise-driven transitions in physics, chemistry, and complex systems. In the classical setting of Gaussian diffusion, the mean escape time typically decreases monotonically with increasing noise intensity, in line with Kramers-type physics (Kramers 1940). Over the years, however, a number of nonequilibrium scenarios have shown that the lifetime of a metastable state can be enhanced by noise over an intermediate range of intensities, producing a pronounced maximum of a suitable mean time scale. This counterintuitive behavior is usually discussed under the denomination of noise-enhanced stability (NES) (Agudov and Spagnolo 2001; Dubkov et al. 2004; Fiasconaro et al. 2005; Hurtado et al. 2006).

A natural question is how these ideas change when the driving fluctuations are non-Gaussian and dominated by rare large events. A canonical model is provided by symmetric  $\alpha$ -stable Lévy flights, whose increments have heavy tails and allow arbitrarily long jumps. Such processes appear in many contexts and admit complementary descriptions, namely a Langevin equation driven by Lévy white noise, and a fractional Fokker–Planck equation with a nonlocal space derivative (Lévy 1937; Gnedenko and Kolmogorov 1954; Metzler and Klafter 2000; Dubkov et al. 2008). In barrier-crossing problems, Lévy flights can modify the notion of activation because a single large jump may overcome the barrier region, and stationary measures may deviate from the usual Gibbs form (Chechkin et al. 2005, 2007; Dybiec et al. 2007; Imkeller et al. 2009, 2010). In barrier-crossing problems, Lévy flights can overcome the barrier through rare long jumps, so that escape is not solely governed by diffusive exploration up to the barrier top, as in the Gaussian case (Chechkin et al. 2005, 2007; Dybiec et al. 2007; Imkeller et al. 2009, 2010).

Lévy flights and, more generally,  $\alpha$ -stable fluctuations provide a standard modeling route for dynamics dominated by rare large increments (Dubkov et al. 2008; Zaburdaev et al. 2015). Within condensed-matter and material settings, Lévy-type statistics have been discussed in charge and phase-transport problems, including graphene-related platforms, as a possible mechanism behind impulsive, non-thermal switching events (Briskot et al. 2014; Gattenlöchner et al. 2016; Guarcello et al. 2017b; Kiselev and Schmalian 2019; Fonseca et al. 2023, 2024). Signatures consistent with heavy-tailed fluctuations have also been reported in optical and semiconductor contexts, from photoluminescence in doped samples and interstellar scintillation to transport and optical response in nanocrystal quantum dots (Luryi and Subashiev 2010; Semyonov

et al. 2012; Subashiev et al. 2014; Boldyrev and Gwinn 2003, 2005; Boldyrev and Konigl 2006; Gwinn 2007; Novikov et al. 2005; Kuno et al. 2000, 2001; Shimizu et al. 2001; Messin et al. 2001; Brokmann et al. 2003). Beyond these examples,  $\alpha$ -stable noise models are routinely used in applied settings where impulsive disturbances and outliers are relevant, including quasiballistic heat conduction, telecommunications and network interference, and vibration-based condition monitoring (Vermeersch et al. 2015a,b; Mohammed et al. 2015; Upadhyaya and Aksamija 2016; Yang and Petropulu 2003; Bhatia et al. 2006; Cortes et al. 2010; Tsihrintzis and Nikias 1995; Subramanian et al. 2015; Shongwe et al. 2015; Karakus et al. 2020; Li and Yu 2010; Chouri et al. 2014; Saadane et al. 2015; Elyassami et al. 2016; White 1984; McFadden and Smith 1984). In this direction, Josephson-based threshold detection schemes have been proposed to access non-Gaussian,  $\alpha$ -stable, current fluctuations by leveraging the sensitivity of switching/escape observables to rare, large excursions (Guarcello et al. 2019, 2020; Guarcello 2021; Guarcello et al. 2024a). More broadly, heavy-tailed jump statistics have also been discussed in other application areas, including geophysical and climate variability, biological motion and search, and financial time series; in those cases the main commonality is the presence of intermittency and rare, high-impact events, rather than a shared microscopic mechanism.

More broadly, Lévy-type statistics have been discussed and used as effective models in biological motion and search (West and Deering 1994; Brockmann et al. 2006; Sims et al. 2008; Reynolds 2009) and in financial time series (Mantegna and Stanley 1995). Related heavy-tailed descriptions have also been considered in geophysical and atmospheric variability (Shlesinger et al. 1995; Ditlevsen 1999), where the common theme is intermittency and rare, high-impact events rather than a shared microscopic mechanism.

In this section, we discuss the framework to quantify metastable trapping under symmetric Lévy noise using residence-time observables (Dubkov et al. 2025). Rather than focusing exclusively on first-passage events, we consider the mean residence time (MRT) within a given interval, which provides a robust measure of how long trajectories spend inside a prescribed observation window. A key advantage is that the MRT can be derived from the fractional transport equation without imposing high-barrier or weak-noise approximations. We then specialize to the analytically tractable case of Cauchy noise ( $\alpha = 1$ ) in a cubic metastable potential, where an explicit quadrature formula for the MRT can be obtained and used to demonstrate a finite, nonmonotonic NES-like behavior.

## 2.1 Model

We consider an overdamped particle in a smooth potential  $V(x)$  under symmetric  $\alpha$ -stable Lévy noise,

$$\frac{dx}{dt} = -V'(x) + L_\alpha(t), \quad 0 < \alpha < 2, \quad (1)$$

where  $L_\alpha(t)$  is a white Lévy noise source (Dubkov and Spagnolo 2005; Dubkov et al. 2008). The transition probability density  $P(x, t|x_0, 0)$  obeys the fractional Fokker–Planck equation

$$\frac{\partial P}{\partial t} = \frac{\partial}{\partial x} [V'(x) P] + D_\alpha \frac{\partial^\alpha P}{\partial |x|^\alpha}, \quad (2)$$

where  $D_\alpha$  sets the noise intensity, with typical spread  $(D_\alpha t)^{1/\alpha}$ , and  $\partial^\alpha/\partial|x|^\alpha$  is the Riesz fractional derivative (Metzler and Klafter 2000; Jespersen et al. 1999; West et al. 1997; Yanovsky et al. 2000).

To quantify metastable trapping, we introduce an observation window  $(L_1, L_2)$  and define the residence time (Dubkov et al. 2020)

$$T(x_0) = \int_0^\infty 1_{(L_1, L_2)}(x(t)) dt, \quad (3)$$

with

$$1_{(L_1, L_2)}(y) = \begin{cases} 1, & y \in [L_1, L_2], \\ 0, & \text{otherwise.} \end{cases} \quad (4)$$

The corresponding MRT is

$$\tau_{\text{MRT}}(x_0) = \langle T(x_0) \rangle = \int_0^\infty dt \int_{L_1}^{L_2} P(x, t|x_0, 0) dx. \quad (5)$$

Operationally,  $\tau_{\text{MRT}}$  measures how strongly the metastable region traps stochastic trajectories. For a purely deterministic overdamped dynamics (no noise), the MRT either reduces to a deterministic transit time, if the trajectory crosses the interval, or becomes ill-defined when deterministic barrier crossing is impossible. In contrast, under Lévy noise, rare long jumps can produce barrier crossing even at very small noise intensities, which makes the small-noise behavior of  $\tau_{\text{MRT}}$  quite different from the Gaussian case.

A successful strategy is to introduce the time-integrated propagator  $Z(x, x_0) = \int_0^\infty P(x, t|x_0, 0) dt$ . Integrating Eq. (2) over time yields an exact equation for  $Z$  (Dubkov et al. 2025),

$$\frac{d}{dx} [V'(x) Z] + D_\alpha \frac{d^\alpha Z}{d|x|^\alpha} = -\delta(x - x_0), \quad (6)$$

which can be analyzed efficiently in Fourier space. This approach leads to closed expressions for  $\tau_{\text{MRT}}(x_0)$  in terms of auxiliary functions defined by the Fourier-transformed problem (see Dubkov et al. (2025) for further details).

## 2.2 Results

The final closed expression for  $\tau_{\text{MRT}}(x_0)$  and the differential equation for the auxiliary function  $G(k, z)$ , defined as the derivative with respect to  $x_0$  of the Fourier transform of the function  $Z(x, x_0)$ , are given by

$$\tau_{\text{MRT}}(x_0) = \int_{x_0}^\infty \text{Re} \left\{ \int_0^\infty G(k, z) \frac{e^{-ikL_2} - e^{-ikL_1}}{\pi ik} dk \right\} dz, \quad (7)$$

and

$$V' \left( -i \frac{d}{dk} \right) G - i D_\alpha k^{\alpha-1} G = \exp^{ikx_0}. \quad (8)$$

These equations (7) and (8) are the exact relations useful to calculate the MRT of a symmetric Lévy flights with arbitrary index  $\alpha$  and noise intensity parameter  $D_\alpha$  in a smooth potential profile with a sink at  $x = \infty$ .

A generic metastable potential can be modeled by the cubic form

$$V(x) = -\frac{x^3}{3} + m^2 x, \quad (9)$$

which exhibits a local minimum at  $x = -m$  and a barrier top (local maximum) at  $x \equiv x_m = +m$  with  $m > 0$ . We focus on the Cauchy case  $\alpha = 1$ , which is analytically tractable while still capturing the hallmark feature of Lévy flights, namely heavy-tailed jumps. In this case, the Fourier-space problem reduces to a linear ordinary differential equation and yields an explicit expression for the MRT in quadratures

$$\begin{aligned} \tau_{\text{MRT}}(x_0) = & \frac{D_1}{\pi} \int_{x_0}^\infty \left[ A \left( \frac{z + \lambda_2}{\lambda_1} \right) + B \right] \frac{dz}{(z^2 - m^2)^2 + D_1^2} \\ & + \frac{D_1}{\pi} \int_{x_0}^\infty \ln \left| \frac{z - L_1}{z - L_2} \right| \frac{dz}{(z^2 - m^2)^2 + D_1^2} \\ & + \int_{x_0}^{L_2} \frac{(z^2 - m^2) dz}{(z^2 - m^2)^2 + D_1^2}, \end{aligned} \quad (10)$$

with

$$A = \arctan \frac{\lambda_2 + L_2}{\lambda_1} - \arctan \frac{\lambda_2 + L_1}{\lambda_1}, \quad (11)$$

$$B = \frac{1}{2} \ln \frac{\lambda_1^2 + (L_2 + \lambda_2)^2}{\lambda_1^2 + (L_1 + \lambda_2)^2}, \quad (12)$$

and  $\lambda = \lambda_1 + i\lambda_2$  depending on  $(m, D_1)$  through the complex root structure of the Cauchy-driven problem (Dubkov et al. 2025). The equations (7), (8) and (10) are the main results of this study.

Equation (10) provides an operational link between a measurable time scale,  $\tau_{\text{MRT}}(x_0)$ , and the control

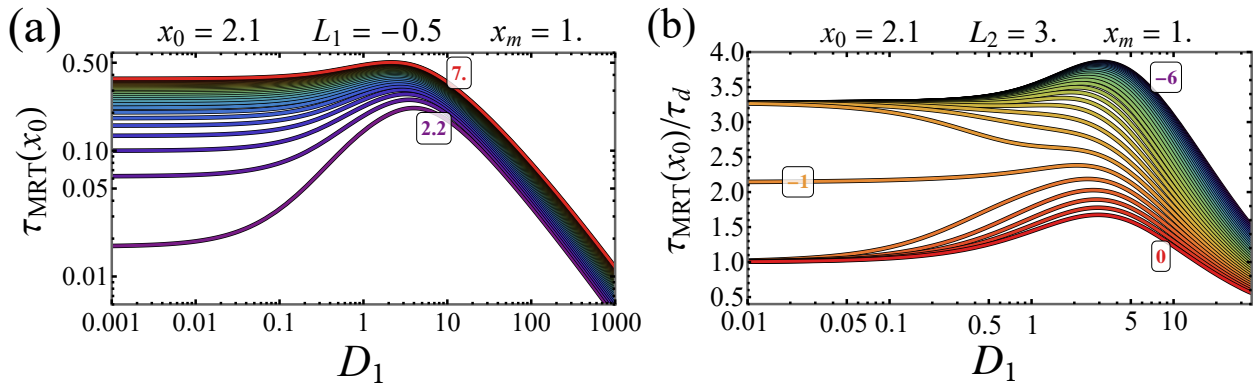


**Figure 1.** MRT for Cauchy noise ( $\alpha = 1$ ) in the cubic metastable potential  $V(x) = -x^3/3 + m^2x$  with  $m = x_m = 1$  and initial condition  $x_0 = 2.1$ . (a) MRT  $\tau_{\text{MRT}}(x_0)$  versus noise intensity  $D_1$  for  $L_1 = -0.5$  and  $L_2 \in [2.2, 7]$  in steps of 0.2 (log-log scale,  $D_1 \in [10^{-3}, 10^3]$ ), highlighting the NES maximum and the large- $D_1$  power-law decay. (b) Normalized MRT  $\tau_{\text{MRT}}(x_0)/\tau_d(x_0)$  versus  $D_1$  for  $L_2 = 3$  and  $L_1 \in [-6, 0]$  in steps of 0.2, showing the NES maximum for all explored  $L_1$  and the characteristic ‘duck-bill’ structure associated with boundary-controlled trapping under Lévy flights. Here  $\tau_d(x_0)$  denotes the deterministic transit time to  $L_2$  for the noiseless overdamped dynamics, when this time is finite.

parameters,  $D_1$  and  $(L_1, L_2)$ . The systematic feature is a finite nonmonotonic dependence of  $\tau_{\text{MRT}}$  on  $D_1$ , with a pronounced maximum over an intermediate range of noise intensities, see Fig. 1. This maximum represents the NES signature for heavy-tailed fluctuations. A compact physical picture is based on competing contributions: increasing  $D_1$  promotes repeated entry and re-entry into the metastable region, which increases the accumulated residence time, while larger  $D_1$  also increases the incidence of long jumps that eject trajectories rapidly from the sink, which reduces residence.

A practical point is that the NES nonmonotonicity of the mean residence time persists over broad parameter ranges and remains well defined within the chosen observation window. In particular, rare long jumps provide an additional pathway for leaving (and re-entering) the region, so the small-noise behavior and the very meaning of ‘residence’ depend explicitly on how the interval boundaries are set. This dependence becomes particularly transparent when  $\tau_{\text{MRT}}$  is scanned versus  $D_1$  while varying either  $L_2$  at fixed  $L_1$ , or  $L_1$  at fixed  $L_2$ .

The two-panel representation in Fig. 1 is a convenient summary of boundary-controlled trapping. Panel (a) shows  $\tau_{\text{MRT}}(x_0)$  versus  $D_1$  for a family of right boundaries  $L_2$  at fixed  $L_1$ . In this plot, varying  $L_2$  changes the effective distance to absorption and therefore the weight of long-jump exits, while keeping the left boundary fixed. The persistence of an NES maximum across the explored  $L_2$  range indicates that the enhancement is not tied to a single geometric choice, and the log-log scale makes the large- $D_1$  power-law decay directly visible.

Panel (b) focuses on the normalized observable  $\tau_{\text{MRT}}(x_0)/\tau_d(x_0)$  at fixed  $L_2$  while scanning the left

boundary  $L_1$ . Here,  $\tau_d(x_0)$  denotes the deterministic transit time to the right boundary in the noiseless overdamped dynamics. It is worth noting that both the maxima and the overall magnitude of the curves increase as the left boundary  $L_1$  is shifted to smaller values, i.e., as the basin of attraction of the metastable state is enlarged, leading to an increase in the normalized MRT (Dubkov et al. 2025). The resulting family of curves displays the characteristic ‘duck-bill’ profile previously reported by Dubkov et al. (2025), with the NES maximum systematically shifting as  $L_1$  is varied. This behavior can be interpreted as a boundary-controlled crossover between a regime in which trajectories spend long times repeatedly returning to the well region, and a regime in which long jumps dominate the escape dynamics, effectively washing out the influence of the metastable basin.

Two limiting behaviors provide useful scaling intuition. For large noise intensities, the MRT follows a power-law decay,

$$\tau_{\text{MRT}}(x_0) \sim D_1^{-1}, \quad (13)$$

consistent with escapes dominated by frequent large jumps and with the broader landscape of Lévy-driven barrier crossing (Chechkin et al. 2005, 2007). In the opposite limit  $D_1 \rightarrow 0$ , the MRT approaches finite, boundary-dependent values, reflecting the fact that rare but finite-probability long jumps can still induce barrier crossing even at vanishing noise intensity.

Overall, the MRT framework provides a clear and robust characterization of metastable trapping under Lévy flight dynamics. General equations enabling the exact calculation of the MRT for superdiffusive processes with arbitrary stability index  $\alpha$  and arbitrary potential landscapes have

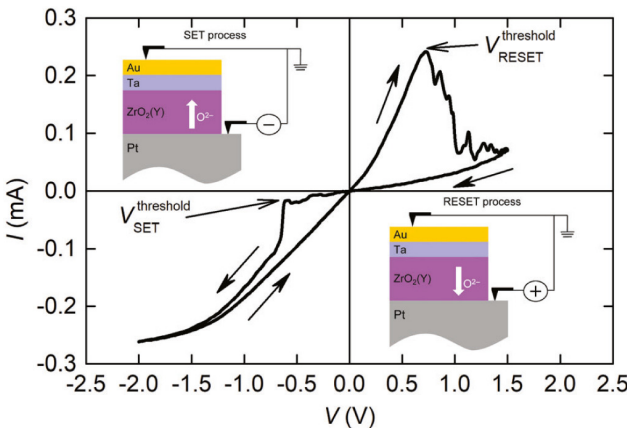


**Figure 2.** Typical I-V curve of a memristive device based on a Ta/ZrO<sub>2</sub>(Y)/Pt stack. The direction of the voltage sweep is shown by arrows. Inset: schematic representation of the oxygen ions drift under the action of an electric field in different directions. From [Koryazhkina et al. \(2022\)](#).

been derived. In particular, the Cauchy case represents a rare setting in which non-Gaussian barrier crossing can be analyzed without uncontrolled approximations, and in which an NES enhancement naturally emerges in a form that is directly linked to experimental measurement protocols and boundary conditions.

### 3 Switching dynamics in memristors

Memristors are nonlinear, history-dependent two-terminal devices whose instantaneous resistance, memristance, depends on the time integral of the applied voltage or current, thereby providing an intrinsic mechanism for nonvolatile memory. Originally postulated by Chua as the fourth fundamental circuit element linking charge and magnetic flux ([Chua 1971](#)), the memristor completes the symmetry among the fundamental circuit variables. The modern physical realization of memristive behavior was experimentally demonstrated by [Strukov et al. \(2008\)](#) in TiO<sub>2</sub>-based nanoscale devices, where resistance switching emerges from field-driven ionic transport and the formation of conductive filaments. From a dynamical-systems perspective, memristive systems are governed by coupled nonlinear equations with internal state variables, leading to a rich variety of phenomena, including hysteresis in the current–voltage characteristics, multistability, threshold dynamics, strong nonlinearity, and resistive switching (RS) between low-resistance (LRS) and high-resistance (HRS) states (see Fig. 2).

These properties underpin the suitability of memristors for neuromorphic architectures, where they can emulate synaptic plasticity mechanisms. Moreover, their scalability to the nanoscale, low-energy switching, and compatibility

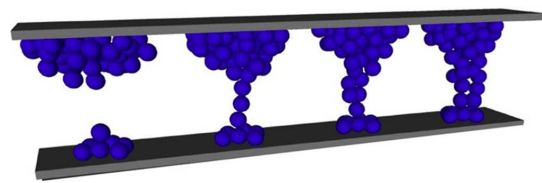


**Figure 3.** A filament growth model for resistive random access memory switching.

with CMOS technologies make memristors promising candidates for high-density nonvolatile memories and in-memory computing platforms ([Yang et al. 2013](#)).

Over the past two decades, resistive switching in memristive devices has attracted significant research attention ([Shi et al. 2021](#); [Sun et al. 2019](#)). Resistive switching (RS) refers to the bistable—or more generally multistable—transition of the resistance of a thin dielectric film sandwiched between two conductive electrodes under the application of an external voltage. To date, the prevailing understanding of the RS mechanism is largely based on the filamentary model, which attributes switching to the formation (set) and rupture (reset) of conductive filaments (CFs) connecting the electrodes within the functional dielectric layer under an applied electric field ([Sun et al. 2019](#)).

In oxide-based memristive devices, conductive filaments are primarily composed of chains of oxygen vacancies. Memristors are therefore regarded as promising candidates for a wide range of applications, including nonvolatile resistive random access memory (RRAM), emerging computing architectures, and neuromorphic electronic circuits ([Yu 2016](#); [Khan et al. 2021](#); [Chua et al. 2022](#); [Li et al. 2018](#); [Boyat et al. 2018](#); [Guo et al. 2022](#); [Pi et al. 2019](#); [Wang et al. 2021c, 2019, 2021b](#); [Lv et al. 2018](#); [Mahata et al. 2020](#); [Wang et al. 2021a](#); [Lv et al. 2020](#); [Huang et al. 2021](#); [Yu et al. 2013](#); [Kim et al. 2015](#); [Hussain et al. 2019](#); [Mikhaylov et al. 2020](#); [Resheed et al. 2021](#); [Kousar et al. 2021](#); [Alsuwian et al. 2021](#); [Rasheed et al. 2021](#); [Khera et al. 2022](#); [De Stefano et al. 2024](#)). However, progress toward practical deployment is currently limited by the insufficient stability and reproducibility of resistive switching (RS) parameters during device operation ([Alonso et al. 2021](#); [Ielmini and Waser 2016](#); [Wu et al. 2014](#)).

Although substantial advances have been achieved in recent years, the overall performance of memristive devices remains inadequate for most large-scale applications. A key challenge is the intrinsically stochastic nature of the RS process, which constitutes a fundamental property of filament formation and rupture and leads to variability in switching voltages, resistance states, and device endurance ([Koryazhkina et al. 2022](#)).

The stochastic nature of resistive switching has been widely observed and analyzed in the literature ([Lee et al.](#)

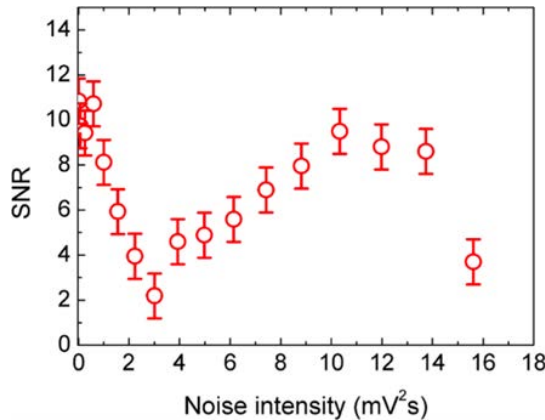


**Figure 4.** Memristance SNR vs. noise intensity experimentally obtained for the memristive device under study.

From [Mikhaylov et al. \(2021\)](#).

2015; Frick et al. 2022; Stotland and Di Ventra 2012; Gaba et al. 2013; Naous et al. 2016; Guarcello et al. 2017a; Filatov et al. 2019; Ntinas et al. 2019; Naous et al. 2021; Ntinas et al. 2021; Wang et al. 2022; Patterson et al. 2013). In this context, a novel strategy for improving memristor stability has recently been proposed. This approach treats the memristor as a multistable stochastic system and exploits well-established phenomena associated with the constructive role of noise in such systems. Within this framework, the device dynamics can be effectively described by a model of overdamped Brownian motion in a multistable force landscape, as proposed in [Agudov et al. \(2020\)](#).

Several phenomena characteristic of multistable stochastic systems have been experimentally observed and theoretically investigated in memristive devices, including stochastic resonance ([Mikhaylov et al. 2021](#)), resonant activation, and transient bimodality ([Koryazhina et al. 2022](#)). In particular, stochastic resonance has been studied both experimentally and theoretically in a metal-oxide memristive device based on yttria-stabilized zirconium dioxide and tantalum pentoxide, which exhibits bipolar filamentary resistive switching of anionic type. The effect of additive white Gaussian noise superimposed on a subthreshold sinusoidal driving signal was analyzed using time-series statistics of the resistive switching parameters, spectral response to periodic perturbations, and the output signal-to-noise ratio of the nonlinear system (see Fig. 4).

These studies revealed stabilized resistive switching and an enhanced memristive response at an optimal noise intensity, consistent with the occurrence of stochastic resonance. The results were interpreted using a stochastic memristor model that explicitly accounts for an external noise source added to the control voltage. Overall, these findings clearly demonstrate that noise and fluctuations can

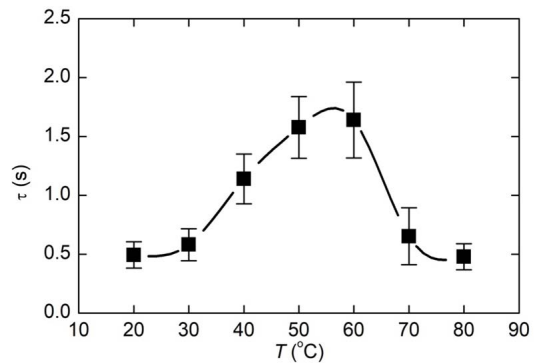


**Figure 5.** Temperature dependence of the relaxation time of the memristor during the switching from LRS to HRS. From [Filatov et al. \(2022\)](#).

play a constructive role in nonlinear memristive systems far from equilibrium ([Mikhaylov et al. 2021](#)).

The phenomenon of noise-enhanced stability (NES) provides another striking example of the beneficial role of noise in stochastic nonlinear systems. The escape time  $\tau$  of a Brownian particle in a fluctuating metastable state was investigated by [Agudov et al. \(2003\)](#) and [Dubkov et al. \(2004\)](#), where its dependence on the fluctuation intensity  $D$  was shown to be nonmonotonic, exhibiting a maximum at an intermediate value of  $D$ . More recently, this effect has been observed experimentally in memristive devices ([Filatov et al. 2022](#)). In that study, the kinetics of resistive switching (RS) during the transition from the low-resistance state (LRS) to the high-resistance state (HRS) was investigated as a function of temperature, which serves as a measure of the internal (thermal) noise intensity. The relaxation time  $\tau$  displayed a nonmonotonic dependence on temperature, with a pronounced maximum. These experimental results were interpreted as evidence of the NES effect in memristors and constitute the first observation of noise-enhanced stability in memristive devices driven by thermal noise (see Fig. 5).

Very recently, a nonmonotonic dependence of the relaxation time in a  $\text{ZrO}_2(\text{Y})$ -based memristive device was observed during switching from the low-resistance state (LRS) to the high-resistance state (HRS) as a function of the intensity of an externally applied noise signal. The observed resistive switching kinetics exhibits at least two distinct regimes: a fast switching process from the LRS to an intermediate state with higher resistance, followed by a slower relaxation toward the stationary HRS. The occurrence of fast switching at random times is a hallmark of transient bimodality, a phenomenon that has been theoretically investigated in memristive systems using the model of overdamped Brownian motion in a multistable potential landscape ([Agudov et al. 2020](#); [Koryazhina et al. 2022](#)). From a physical perspective, the fast switching

regime corresponds to the initial rupture of the conductive filament.

The dependence of the relaxation time  $\tau$  on the external noise intensity  $\theta_\zeta$  is shown in Fig. 6. The behavior is clearly nonmonotonic, with a maximum occurring at  $\theta_\zeta \approx 6.1 \cdot 10^{-9} \text{ V}^2\text{s}$ . A simple stochastic model describing the dynamics of such a memristive device is based on a Langevin equation that accounts for the random hopping of a positively charged oxygen vacancy between trapping sites in the dielectric layer (Agudov et al. 2020)

$$\frac{dx}{dt} = -\frac{\partial \Phi(x)}{\partial x} + F + \xi(t), \quad (14)$$

where  $x$  is the coordinate of the hopping particle,  $\xi(t)$  is a white Gaussian noise with statistical properties  $\langle \xi(t) \rangle = 0$  and  $\langle \xi(t)\xi(t+t') \rangle = 2\theta_\xi \delta(t')$ , with  $\theta_\xi = \eta k_B T$ , where  $k_B$  is Boltzmann constant,  $\eta$  is viscosity coefficient according to the Sutherland–Einstein relation, and  $T$  is the temperature. The potential landscape experienced by the hopping particle is modeled as a periodic potential  $\Phi(x)$ , consisting of potential wells separated by barriers of height  $E_a$ , corresponding to the activation energy. The particle dynamics is influenced by both the internal microstructure of the device and the externally applied electric field. The electric force acting on the particle is taken to be proportional to the applied voltage  $F = qV/L$ , where  $q$  is the particle charge and  $L$  is the effective distance between electrodes. If an additive noise source  $\zeta(t)$  is applied to the driving voltage, the total voltage becomes

$$V = V_0 + \zeta(t), \quad (15)$$

which leads to a stochastic modulation of the force term in Eq. (14), obtaining

$$\begin{aligned} \eta \frac{dx}{dt} &= -\frac{\partial \Phi(x)}{\partial x} + \frac{q}{L} V_0 + \frac{q}{L} \zeta(t) + \xi(t) \\ &= -\frac{\partial \Phi(x)}{\partial x} + \frac{q}{L} V_0 + \nu(t), \end{aligned} \quad (16)$$

where the total effective white Gaussian noise acting on the system is  $\nu(t) = (q/L)\zeta(t) + \xi(t)$  with corresponding noise intensity  $\theta_\nu = (q/L)^2\theta_\zeta + \theta_\xi$ . In our experiment  $\zeta(t)$  is a Gaussian noise with zero mean  $\langle \zeta(t) \rangle = 0$  and noise intensity  $\theta_\zeta = \sigma^2 \tau_{\text{corr}}$ , where  $\sigma^2$  is the variance and  $\tau_{\text{corr}}$  is the correlation time. For such a system, it has been theoretically demonstrated that the relaxation time can exhibit a nonmonotonic dependence on the noise intensity (Agudov et al. 2020)

$$\tau(\theta_\nu) = \left( \frac{L^2}{D_{\text{eff}}} \right) \cdot \left[ \frac{1}{\pi^2 + \gamma^2} \right], \quad (17)$$

which includes the effective diffusion coefficient  $D_{\text{eff}}$ , the Kramers time  $\tau_{\text{kr}} = \tau_0 \exp[E_a/\theta_\nu]$ , and the dimensionless parameter  $\gamma = (v_{\text{eff}} L)/(2D_{\text{eff}})$ , with  $v_{\text{eff}}$  the effective drift

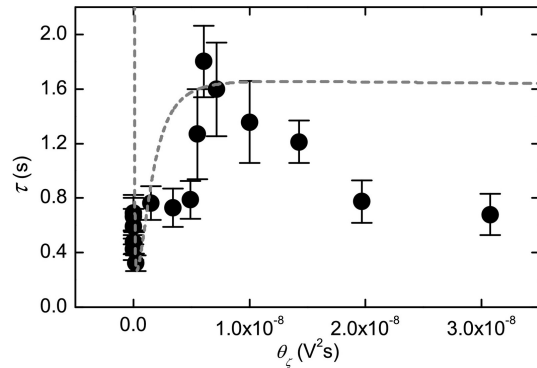


**Figure 6.** Theoretical (dashed gray line) and experimental (black dots) dependencies of the relaxation time from LRS into HRS as a function of the external noise intensity  $\theta_\zeta$ . From Koryazhina et al. (2022).

coefficient. Explicit expressions for these quantities are provided in Koryazhina et al. (2022). We assume that the temperature remains constant throughout the experiment; consequently, the thermal noise intensity can be treated as constant. The theoretical dependence of the relaxation time  $\tau$  (Eq. (17)) on the external noise intensity  $\theta_\zeta$  is shown in Fig. 6 as a dashed gray curve Agudov et al. (2020), together with the experimental data (black dots). The agreement between theory and experiment is quite good, particularly with regard to the nonmonotonic behavior and the presence of a clear maximum in both curves.

This work provides the first experimental evidence of the noise-enhanced stability (NES) effect in the relaxation time dynamics of a memristive device induced by an external noise source. By contrast, the first experimental observation of NES in memristors driven by thermal (internal) noise was reported only very recently (Filatov et al. 2022). These findings highlight the constructive role of both internal and external noise sources and point to their potential use as novel mechanisms for controlling resistive switching dynamics. In practical terms, externally applied noise offers a particularly attractive control strategy, as it can be more easily tuned and implemented to improve the stability and reproducibility of resistive switching.

#### 4 Noise enhanced phenomena in a quantum bistable system

In this section, we explore the role of external driving in the escape dynamics of quantum metastable states under the influence of dissipation (Valenti et al. 2015, 2018). Understanding how a quantum system transitions out of a metastable state is crucial for a range of applications, from quantum information processing to condensed matter physics. In particular, the interplay between monochromatic driving and system–environment coupling can lead to

complex behaviors. We find that, for appropriately chosen driving amplitudes, the escape time exhibits resonant peaks and dips as a function of the driving frequency when the dissipation is relatively weak. As the coupling strength increases, the escape time reaches a pronounced maximum, followed by a rapid decline at a critical value of the coupling. This behavior marks a crossover to a regime in which the escape time becomes essentially independent of the driving frequency, closely resembling the behavior observed in the static (undriven) case. These results highlight the rich dynamics arising from the combined effects of driving and dissipation in quantum metastable systems.

#### 4.1 Caldeira-Leggett model

A paradigmatic example of a quantum dissipative system is given by the Caldeira-Leggett model (Caldeira and Leggett 1983), in which a system  $S$  with generalized coordinate  $\vec{x}$  is coupled to a dissipative environment, represented by a heat bath of quantum harmonic oscillators with frequencies  $\omega_j$  and coordinates  $\vec{x}_j$  through the Hamiltonian

$$\hat{H}(t) = \hat{H}_S(t) + \frac{1}{2} \sum_{j=1}^N \left[ \frac{\hat{p}_j^2}{m_j} + m_j \omega_j^2 \left( \hat{x}_j - \frac{c_j \hat{x}}{m_j \omega_j^2} \right)^2 \right] \quad (18)$$

with  $H_S(t)$  accounting for the presence of a time-varying potential. The second term on the right-hand side of Eq. ((18)) contains the free bath Hamiltonian, the bilinear interaction term between  $S$  and the oscillators, and a renormalization term, dependent on  $\vec{x}$ . This term ensures a purely dissipative bath, resulting in dissipation that is independent of the coordinate of the central system. The resulting time-dependent Hamiltonian for  $S$  reads

$$\begin{aligned} \hat{H}_S(t) &= \frac{\hat{p}^2}{2M} + V(\hat{x}) - \hat{x} A \sin(\Omega t) \\ &= \hat{H}_0 - \hat{x} A \sin(\Omega t). \end{aligned} \quad (19)$$

where the static potential  $\vec{V}(x)$  is given by

$$V(\hat{x}) = \frac{M^2 \omega_0^4}{64 \Delta U} \hat{x}^4 - \frac{M \omega_0^2}{4} \hat{x}^2 - \epsilon \hat{x}. \quad (20)$$

When the bath is assumed to be in thermal equilibrium, its effect on the quantum bistable system is completely described by the Ohmic spectral density Weiss (2012); Magazzù (2015).

#### 4.2 Discrete variable representation

At low temperatures, relative to the energy scale set by  $\omega_0$ , the particle's time evolution is effectively restricted to a reduced Hilbert space spanned by the first  $M$  energy eigenstates  $|E_i\rangle$ , provided that the particle is not initially

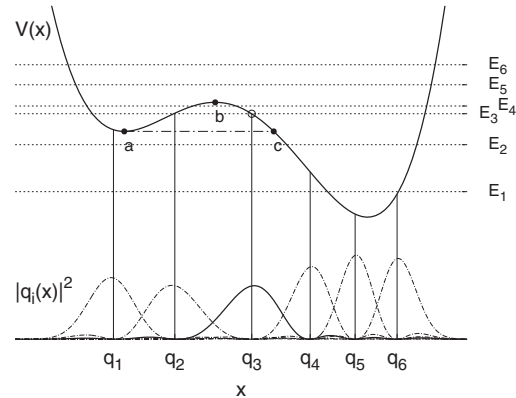


**Figure 7.** Potential  $V$  [Eq. (3), with  $\Delta U = 1.4 \hbar \omega_0$  and  $\epsilon = 0.27 \sqrt{M \hbar \omega_0^3}$ ] and the first six energy levels (horizontal lines). In the lower part, the probability densities  $|q_i(x)|^2 = |\langle x | q_i \rangle|^2$  associated with the DVR eigenfunctions are shown, the initial state  $|q_3\rangle$  being highlighted by a solid line. Vertical lines indicate the position eigenvalues in the DVR. The metastable region of the potential is to the left of the so-called *exit point*  $c$ . From Valenti et al. (2018).

excited to levels above  $M$ . We further assume that the time-dependent driving does not induce transitions to energy eigenstates beyond those already considered in the static potential. In addition, these energy eigenstates are the same as those of the system described by  $\hat{H}_0$  in Eq. (2). Moreover, when the frequency of the periodic external driving is comparable to or larger than the energy gap between the ground state and the first excited state,  $\Omega \geq \omega_0$ , it is appropriate to average the dynamics over a full driving period (Grifoni and Hänggi 1998; Thorwart et al. 2000, 2001). After this averaging, the resulting transition coefficients become time-independent, forming the time-averaged rate matrix. If the driving frequency does not satisfy this high-frequency condition, Floquet theory provides an alternative theoretical framework.

The populations  $\rho_{jj}$  of the discrete variable representation (Feynman and Vernon 1963; Harris et al. 1965; Light and Carrington 2007) (DVR) states  $|q_j\rangle$  relax toward a stationary configuration that depends on the bath parameters and the damping strength  $\gamma$ . Consequently, at strong coupling, this relaxation process is well described by the incoherent dynamics governed by the master equation (Thorwart et al. 2000, 2001; Magazzù 2015)

$$\dot{\rho}_{jj}(t) = \sum_k \Gamma_{jk}^{av} \rho_{kk}(t), \quad (21)$$

with  $\Gamma_{jk}^{av}$  being time-independent averaged rates.

#### 4.3 Escape time for the driven system

We study the transient dynamics of the driven system described by Eq. (21), starting from a nonequilibrium initial

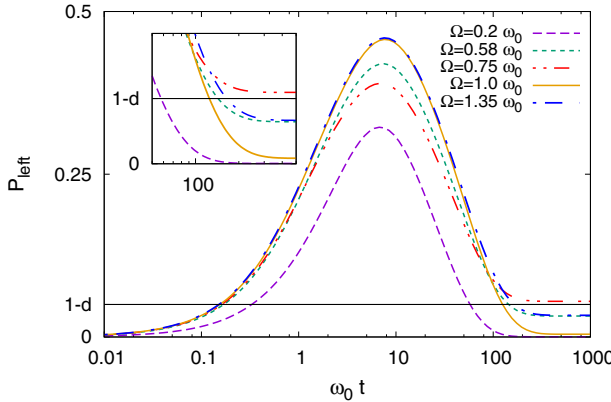


**Figure 8.** Left well population  $P_{left} = \rho_{11} + \rho_{22}$  as a function of time (in log scale) for  $\bar{A} = 0.15$ ,  $\bar{T} = 0.1$ ,  $\gamma/\omega_0 = 0.2$ , and five driving frequency values, namely  $\Omega/\omega_0 = 0.2, 0.58, 0.75, 1.0, 1.35$ . Here we introduced the dimensionless quantities of the amplitude and temperature,  $\bar{A} = A/\sqrt{M\hbar\omega_0^3}$  and  $\bar{T} = k_B T/\hbar\omega_0$ . Horizontal line:  $1-d$ , where  $d = 0.95$  is the threshold value. For  $\Omega/\omega_0 = 0.75$  no escape occurs, as  $P_{left}$  remains above the value  $1-d$ . This is better shown in the inset. Note the nonmonotonic behavior of the steady-state values of  $P_{left}$  as a function of  $\Omega$ . From [Valenti et al. \(2018\)](#).

condition,

$$\rho(0) = |q_3\rangle\langle q_3|, \quad (22)$$

that is, with the particle initially localized in the central region of the potential on the right side of the barrier, between the maximum and the exit point, denoted as  $c$  in Fig. 7. Consequently, the time evolution of the populations in our asymmetric bistable quantum system (see Fig. 8), under the initial condition Eq. (22), is described by

$$\rho_{ij}(t) = \sum_{n=1}^6 S_{jn} (S^{-1})_{n3} e^{\Lambda_n(t-t_0)} \rho_{33}(t_0). \quad (23)$$

We analyze the escape time from the metastable region, defined as the area to the left of the exit point  $c$  in Fig. 7, following [Sargsyan et al. \(2007\)](#), where the decay rate from the metastable region is determined using the probability of a Gaussian wave packet tunneling from left to right across the potential barrier shown in Fig. 7. In the present work, we employ a discretized version of this method. Specifically, we compute the population of the lower (right-side) well, corresponding to the cumulative population of the three DVR states  $|q_4\rangle$ ,  $|q_5\rangle$ , and  $|q_6\rangle$ ,

$$P_{right}(t) = \sum_{j=4}^6 \rho_{jj}(t). \quad (24)$$

We define the escape time  $\tau$  from the metastable region of the potential (the area to the left of the exit point  $c$ ) as the time required for the population of the right well to

reach a threshold value  $d$ . In the static case, [Valenti et al. \(2015\)](#) showed that the nonmonotonic behavior of  $\tau$  as a function of  $\gamma$  and the temperature  $T$  remains robust under small variations of the threshold around 0.9. In the present study, we set the threshold to  $d = 0.95$ , meaning that the particle is considered to have escaped from the metastable region once the probability of finding it in the lower (right) well reaches or exceeds 95%.

It is worth noting that, in the static case, the metastable well can be thermally populated at the steady state. In such a scenario, no escape occurs if the threshold  $d$  is close to unity ([Valenti et al. 2015](#)). As we will show below, a similar situation arises in the driven case for certain driving frequencies  $\Omega$ , particularly at large amplitudes  $A$ , when the left-well population, given by  $P_{left} = \rho_{11} + \rho_{22}$ , remains significantly above zero at the steady state due to the effect of the driving.

An example of this effect is shown in Fig. 8, where, for  $\bar{A} = 0.15$ ,  $\bar{T} = 0.1$ , and  $\gamma/\omega_0 = 0.2$ , the population of the left well is plotted as a function of the time for various driving frequencies, where the dimensionless amplitude  $\bar{A} = A/\sqrt{M\hbar\omega_0^3}$  and temperature  $\bar{T} = k_B T/\hbar\omega_0$ . The stationary value of  $P_{left}$  remains above  $1-d = 0.05$  for  $\Omega/\omega_0 = 0.75$ , indicating that no escape occurs at this driving frequency.

$$\rho_{jj}(t) = \sum_{n,k=1}^M S_{jn} (S^{-1})_{nk} e^{\Lambda_n(t-t_0)} \rho_{kk}(t_0), \quad (25)$$

Our primary objective is to study how the escape time depends on the driving frequency and the coupling strength. To this end, we first fix  $\gamma$  at the value used in Fig. 8, which is the lowest value considered in this work, and plot the escape time as a function of both  $\Omega/\omega_0$  and  $\gamma/\omega_0$  for two different amplitude values,  $\bar{A} = 0.15$  and  $0.20$ , respectively, see Figs. 9 and 10. As  $\gamma$  increases, the peaks and dips of  $\tau$  as a function of the driving frequency gradually smooth out, until  $\tau$  becomes nearly independent of  $\gamma$  as the coupling approaches a critical value  $\gamma_c = 0.75$ . For  $\gamma < \gamma_c$ , high-frequency driving can hinder or enhance the escape process, while for coupling strengths exceeding the critical value  $\gamma_c$ , the escape time no longer depends on the driving frequency and the quantum Zeno effect sets in ([Facchi et al. \(2005\)](#)).

The critical value  $\gamma_c$  defines the onset of a dynamical regime in which the tunneling process responsible for the transfer of the population to the states of the metastable region is suppressed. This occurs because the tunneling dynamics slows down relative to the depletion time scale of the region where the particle is initially localized. Consequently, the probability of finding the particle in the metastable well, starting from the initial condition 22, is effectively zero at all times, as the population is transferred directly from  $|q_3\rangle$  to the states of the right well.

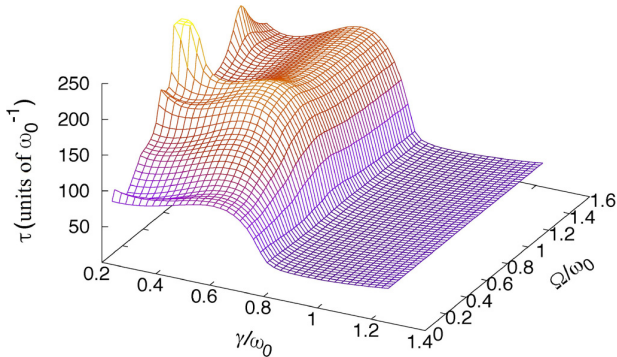


**Figure 9.** Escape time as a function of the coupling strength and the driving frequency for dimensionless amplitudes  $\bar{A} = 0.15$ . The dimensionless temperature is set to the value  $\bar{T} = 0.1$ . From Valenti et al. (2018).

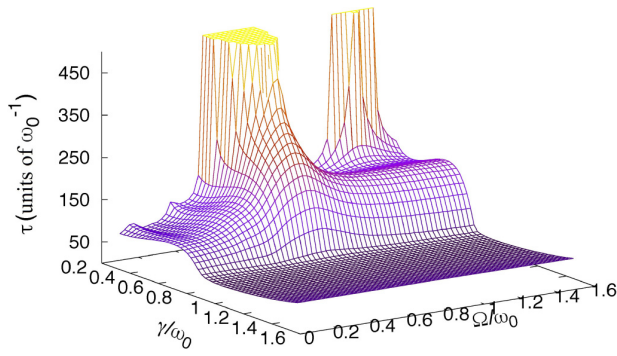


**Figure 10.** Escape time as a function of the coupling strength and the driving frequency for dimensionless amplitudes  $\bar{A} = 0.20$ . The dimensionless temperature is set to the value  $\bar{T} = 0.1$ . From Valenti et al. (2018).

## 5 Axion-Induced Resonant Activation in Josephson Switching Dynamics

We outline a switching-statistics strategy for axion detection using a current-biased Josephson junction (CBJJ) operated as a threshold device. If an axion field couples to the Josephson phase, it can act as an additional weak effective drive and modify the escape dynamics from the superconducting to the finite-voltage state. The central predicted signature is an axion-induced resonant-activation effect, observed as a pronounced minimum in the mean switching time when the tunable junction energy scale is varied. Moreover, a similar structure in the width of the switching-time distributions appears.

### 5.1 Motivation and statistical viewpoint

Josephson junctions, and more broadly superconducting weak-link devices, are widely used as sensitive detectors and readout elements (Barone and Paterno 1982; Devoret

and Schoelkopf 2013; Tafuri 2019; Braginski 2019; Krantz et al. 2019; Citro et al. 2024). They combine strong nonlinearity with low dissipation and low intrinsic noise, and they offer a direct electrical readout in modern superconducting-circuit platforms (Devoret and Schoelkopf 2013; Kjaergaard et al. 2020). In many implementations a JJ acts as a threshold element, where small perturbations (current, magnetic flux, microwave drives, or other weak effective forces on the phase) can produce a pronounced change in the phase dynamics, up to triggering the switch from a metastable superconducting state to a finite-voltage state (Barone and Paterno 1982; Devoret et al. 1984; Guarcello et al. 2016). This “switching-based” strategy is attractive because it can convert weak inputs into measurable large voltage pulses, and it enables statistically robust inference through repeated trials (Devoret et al. 1984; Blackburn et al. 2016; Guarcello and Bergeret 2021; Guarcello et al. 2023, 2024b). Similar ideas underlie a broader landscape of superconducting detectors, including devices operating in regimes relevant to photon and bolometric detection, where low noise and strong nonlinearity are exploited to transduce extremely weak excitations into measurable electrical signals (Chen et al. 2011; Oelsner et al. 2017; Guarcello et al. 2019; Lee et al. 2020; Revin et al. 2020; Walsh et al. 2021; Rettaroli et al. 2021; Pankratov et al. 2025). Moreover, Josephson devices have also been discussed in broader contexts at the interface between superconductivity and axion or axion-like physics, both from the standpoint of particle searches and of axion-electrodynamics-induced Josephson phenomena (Asztalos et al. 2010; Irastorza and Redondo 2018; Nogueira et al. 2016; Kuzmin et al. 2018; Pankratov et al. 2022; Sushkov 2023; Bartram 2023; Braggio et al. 2025).

Within this detector paradigm, a recent and debated line of work has suggested that switching dynamics in a CBJJ could also be sensitive to axion-like dark matter (Beck 2011, 2012, 2013, 2015, 2016). The basic hypothesis is that, under specific conditions, a background axion field may couple to the Josephson phase, thus effectively behaving as an additional time-dependent drive acting on the junction. If such a coupling is present, it should manifest as systematic, reproducible changes in the statistics of escape (switching) events from the superconducting to the resistive state. This provides a basis for a switching-statistics viewpoint as a proposed protocol, in which one would test the hypothesis, i.e., the presence of the axion field, by measuring distributions and their dependence on control parameters, such as mean values and variances, over a large ensemble of switching realizations (Guarcello et al. 2019; Piedjou Komnang et al. 2021; Guarcello et al. 2021).

The proposed framework focuses on switching-time statistics, namely, the time it takes for a junction biased

below its critical current to leave the metastable superconducting state and reach the finite-voltage state (Grimaudo et al. 2022). Under the coupling hypothesis, an axion-induced *resonant activation* (RA) effect may appear as a minimum of the mean switching time (MST), i.e., the average switching time over many independent repeated realizations, as a function of a tunable energy-ratio parameter. This research line is motivated by two considerations. First, the axion misalignment angle obeys an equation of motion that is formally analogous to that of a damped pendulum, and thus resembles the nonlinear equation governing the Josephson phase dynamics in a biased junction (Sikivie 1983; Co et al. 2020). Second, the ratio between the axion and the Josephson energy scales can, in principle, be tuned experimentally. A convenient control parameter is the dimensionless quantity  $\varepsilon = (E_a/\hbar\omega_p)^2$ , where  $E_a = m_a c^2$  (with  $m_a$  the axion mass) and  $\omega_p$  is the Josephson plasma frequency. Since the latter depends on junction parameters and in particular on the critical current (Barone and Paterno 1982), one can scan  $\varepsilon$  by varying the device working conditions, for instance through temperature, magnetic field, or electrostatic gating. This can be done either within a single junction or across an array of junctions with different critical currents (Dubos et al. 2001; Bergeret and Cuevas 2008; Du et al. 2008; De Simoni et al. 2019).

Complementary studies have extended this research framework in two directions. On the one hand, the influence of the axion field has been recast in terms of an effective (quasi)potential barrier governing escape, providing an alternative route to connect switching statistics to an inferred coupling strength (Grimaudo et al. 2023b). On the other hand, in a low-noise quantum limit the coupled dynamics has been discussed in terms of interacting two-level systems, where the axion-like subsystem is indirectly revealed through induced oscillations of an accessible Josephson degree of freedom (Grimaudo et al. 2023a).

In this perspective, if the coupling mechanism assumed in earlier works were realized in a given experimental configuration, one would expect distinctive statistical signatures to emerge in switching-time measurements. In particular, since the term  $\propto \varepsilon \sin \theta$  acts as an effective ac-like drive in the JJ dynamics,  $\langle \tau \rangle(\varepsilon)$  may exhibit RA and develop a minimum when a characteristic axion-JJ oscillation frequency matches the effective plasma frequency of the CBJJ (Grimaudo et al. 2022).

Importantly, one can extend the analysis beyond the mean switching time by tracking the width of the switching-time distribution as well. Similar structures in both mean and dispersion through controlled  $\varepsilon$  scans would provide a more solid and quantitative basis for supporting the axion-coupling hypothesis and for possible experimental validation of the phenomenon.

## 5.2 Josephson phase dynamics and switching statistics

Within the resistively and capacitively shunted junction (RCSJ) description, the Josephson phase  $\varphi$  evolves as a damped particle in a tilted washboard potential (Stewart 1968; McCumber 1968; Barone and Paterno 1982). In normalized units, i.e.,  $\tau_c = \omega_c t$ , with  $\omega_c = (2e/\hbar)I_c R$ , the stochastic equation for a CBJJ reads

$$\beta_c \ddot{\varphi}(\tau_c) + \dot{\varphi}(\tau_c) + \sin \varphi(\tau_c) = i_b + i_n(\tau_c), \quad (26)$$

where overdots denote derivatives with respect to  $\tau_c$ ,  $i_b = I_b/I_c$  is the dc bias current normalized to the critical current  $I_c$ , and  $\beta_c = \omega_c RC$  is the Stewart–McCumber parameter, with  $R$  and  $C$  being the normal-state resistance and capacitance of the JJ, respectively. Thermal fluctuations are modeled as a Gaussian white current noise with  $\langle i_n \rangle = 0$  and

$$\langle i_n(\tau_c) i_n(\tau_c + \tilde{\tau}_c) \rangle = 2\Gamma \delta(\tilde{\tau}_c), \quad (27)$$

where  $\Gamma = \frac{k_B T}{R} \frac{\omega_c}{I_c^2}$  is the dimensionless noise intensity (Barone and Paterno 1982), with  $k_B$  being the Boltzmann constant and  $T$  the temperature. For  $i_b < 1$  the washboard potential hosts metastable minima. Switching corresponds to noise-activated escape over the nearest barrier. The key observables for our purposes are the average value,  $\langle \tau \rangle$ , and the width, i.e., the standard deviation,  $\sigma_\tau$ , of the switching-time distributions.

## 5.3 Axion equation of motion and coupling to a JJ

The axion misalignment angle  $\theta$  obeys, in a homogeneous approximation, to the equation

$$\ddot{\theta}(t) + 3H \dot{\theta}(t) + \frac{m_a^2 c^4}{\hbar^2} \sin \theta(t) = 0, \quad (28)$$

where  $m_a$  is the axion mass and  $H$  is the Hubble parameter (Sikivie 1983; Co et al. 2020).

It is convenient to write the coupled axion–JJ dynamics in normalized units (Grimaudo et al. 2022). Using the characteristic-frequency normalization  $\tau_c = \omega_c t$ , with  $\omega_c = (2e/\hbar)I_c R$ , one obtains the system of stochastic equations

$$\beta_c \ddot{\varphi} + k_2 \dot{\varphi} + k_2 \sin \varphi + k_1 \varepsilon \sin \theta = k_2 (i_b + i_n), \quad (29a)$$

$$\beta_c \ddot{\theta} + k_1 \dot{\varphi} + k_1 \sin \varphi + k_2 \varepsilon \sin \theta = k_1 (i_b + i_n), \quad (29b)$$

where

$$k_1 = \frac{\gamma}{1 + 2\gamma}, \quad k_2 = \frac{1 + \gamma}{1 + 2\gamma}, \quad (30)$$

with  $\gamma$  being the coupling constant between axion and JJ. An axion friction term proportional to  $\dot{\theta}$  is neglected in this model, due to the extremely small ratio  $3H/\omega_p$ . In

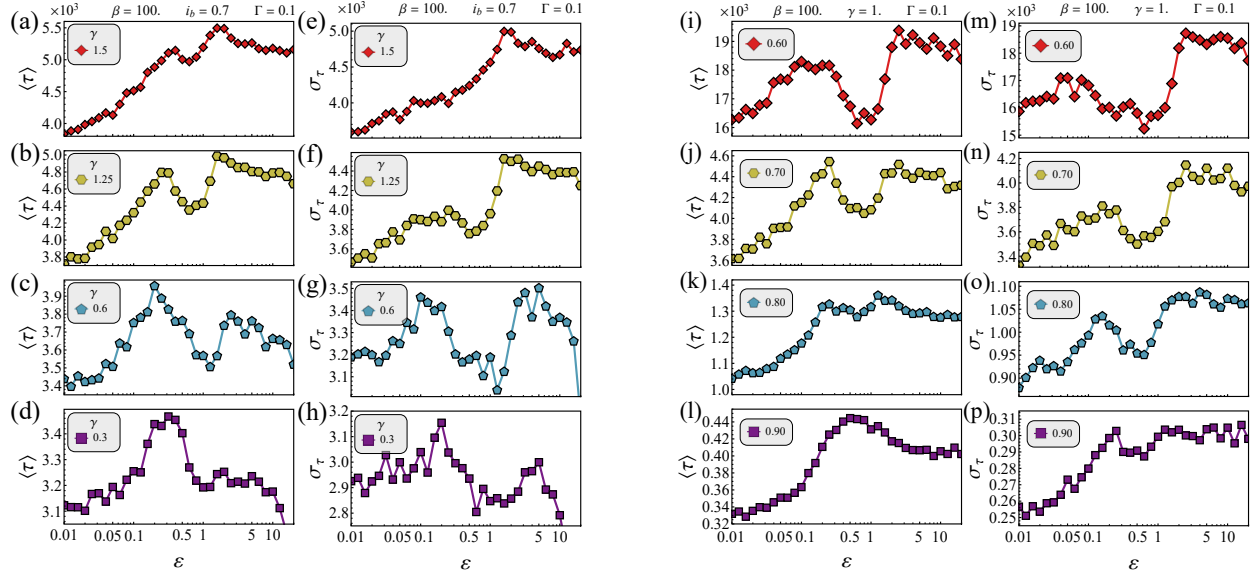


**Figure 11.** Switching-time statistics as a function of the energy-ratio parameter  $\varepsilon$ , for an underdamped junction ( $\beta = 100$ ) at fixed noise intensity  $\Gamma = 0.1$ . Left columns: mean switching time  $\langle \tau \rangle$ , panels (a)–(d), and standard deviation  $\sigma_\tau$ , panels (e)–(h), versus  $\varepsilon$  at fixed coupling  $i_b = 0.7$ , for four axion–JJ coupling values,  $\gamma = 1.5$  (top row), 1.25, 0.6, and 0.3 (bottom row). Right columns: mean switching time  $\langle \tau \rangle$ , panels (i)–(l), and standard deviation  $\sigma_\tau$ , panels (m)–(p), versus  $\varepsilon$  at fixed coupling  $\gamma = 1$ , for four bias values,  $i_b = 0.60$  (top row), 0.70, 0.80, and 0.90 (bottom row).

addition to a dc bias and thermal noise in the JJ branch, the coupling introduces an additional effective term,  $k_1 \varepsilon \sin \theta$ . The central control parameter is the dimensionless *energy ratio*

$$\varepsilon = \left( \frac{m_a c^2}{\hbar \omega_p} \right)^2, \quad \text{with} \quad \omega_p = \sqrt{\frac{2eI_c}{\hbar C}}. \quad (31)$$

A crucial experimental point is that the Josephson plasma frequency is experimentally tunable, because  $I_c$  can be modified in situ by changing the device working point, for instance via temperature, applied magnetic field, or electrostatic gating (Dubos et al. 2001; Bergeret and Cuevas 2008; Du et al. 2008; De Simoni et al. 2019). This makes it possible to scan the energy-scale ratio  $\varepsilon$  in a controlled manner. Operationally, one can scan  $\varepsilon$  either by tuning  $I_c$  in situ in a given device, while keeping  $i_b = I_b/I_c$  in a chosen range, or by using an array of junctions with different  $I_c$  that directly sample different  $\varepsilon$  values.

The system of Eqs. (29) is integrated numerically using an explicit finite-difference scheme with time step  $\Delta t = 10^{-2}$ . Switching-time statistics are then computed over an ensemble of  $10^4$  independent realizations.

## 5.4 Results

Figure 11 shows that, in the underdamped regime ( $\beta = 100$ ) at fixed noise intensity  $\Gamma = 0.1$ , the switching dynamics displays an axion-induced RA effect: the mean switching time becomes a nonmonotonic function of  $\varepsilon$  and

exhibits a clear minimum in the interval  $\varepsilon \in [0.1, 1]$  for intermediate coupling values. Physically, this minimum arises from a frequency-matching condition between the effective Josephson plasma oscillations and the characteristic frequency of the coupled axion–JJ linearized dynamics. The term proportional to  $\varepsilon \sin \theta$  can be interpreted as an oscillating drive acting on the Josephson phase (Grimaudo et al. 2022), with characteristic frequencies obtained from the small-oscillation linearization of the coupled system (noise-free limit). As in standard resonant-activation scenarios, the mean escape time becomes a nonmonotonic function of the control time scale associated with a periodic drive or a time-dependent barrier. When this external time scale approaches the intrinsic oscillation time scales of the metastable dynamics, the escape process is favored, yielding a pronounced minimum in  $\langle \tau \rangle$  as a function of the tuning parameter (Devoret et al. 1984; Doering and Gadoua 1992; Kautz 1996; Guarcello et al. 2015; Ladeynov et al. 2023). In the same regime, one often expects a similar structure in the width of the switching-time distribution, which can be quantified by its standard deviation  $\sigma$ .

Panels (a–d) and (e–h) report, respectively, the mean switching time  $\langle \tau \rangle$  and the standard deviation  $\sigma_\tau$  versus  $\varepsilon$  for several coupling strengths  $\gamma$ , from 0.3 to 1.5, at fixed bias  $i_b = 0.7$ . Changing  $\gamma$  modifies both the switching times and the width of the distribution, and it also affect the visibility of the nonmonotonic structures in  $\varepsilon$ .

The right-hand set of panels focus on the role of the bias current at fixed coupling,  $\gamma = 1$ . In fact, panels (i)–(l) show  $\langle \tau \rangle(\varepsilon)$  for four representative values of  $i_b$ , from 0.6 to 0.9, while panels (m)–(p) show the corresponding  $\sigma_\tau(\varepsilon)$ . A clear and systematic trend is that increasing  $i_b$  reduces the switching times, as expected for escape from a tilted metastable potential, while preserving a pronounced structure versus  $\varepsilon$ . The nonmonotonic features are most visible at lower bias, where the metastable well is deeper and the escape time scale is longer, whereas at higher bias the curves become flatter and the relative modulation is reduced. In the same  $\varepsilon$  region where  $\langle \tau \rangle$  displays a dip,  $\sigma_\tau$  typically shows also a nonmonotonic modulation in the same  $\varepsilon$  window, which is consistent with a reshaping of the full switching-time distribution rather than a simple rigid shift of its mean.

Overall, Fig. 11 provides a compact view of how the proposed signature, i.e., a reduction of the mean switching time due to RA, accompanied by a corresponding feature in the dispersion, depends on both the coupling parameter  $\gamma$  and the operating point set by  $i_b$ .

Two additional qualitative features are emphasized as practical detection tools. First, for  $\varepsilon \ll 1$  the axion term becomes ineffective and Eqs. (29) effectively decouple, so switching statistics approach the unperturbed JJ behavior. Second, for  $\varepsilon \gg 1$  the axion-induced term produces for sufficiently large  $\gamma$  a plateau in the switching-time observables. Therefore, an experimental scan in  $\varepsilon$  can simultaneously test for (i) the presence of an RA minimum near  $\varepsilon \lesssim 1$  and (ii) a statistically significant separation between the small- $\varepsilon$  and large- $\varepsilon$  plateaus. Finally, as discussed by Grimaudo et al. (2022), we stress that the coupling-induced signatures are expected to be most visible in the underdamped regime; for strong damping (small  $\beta_c$ ) the effective coupling becomes negligible, making this mechanism ineffective.

## 6 Conclusions

In this work we have reviewed a collection of recent results that share a common message: metastability in nonlinear systems can be controlled, and in specific regimes even reinforced, by fluctuations, dissipation, and time-dependent perturbations. Starting from Lévy-driven barrier crossing, we emphasized how heavy-tailed noise qualitatively alters escape physics, yielding a finite, boundary-dependent residence-time behavior in the small-noise limit and producing a pronounced nonmonotonic dependence of the mean residence time on the Lévy-noise intensity. This provides a rigorous and measurement-oriented extension of noise-enhanced stability beyond the Gaussian setting.

We then connected these ideas to solid-state devices, focusing on memristors as paradigmatic multistable nonequilibrium systems. In oxide-based filamentary

devices, the intrinsically stochastic nature of resistive switching leads to large variability, but also enables constructive noise-induced phenomena. The experimental evidence of stochastic resonance and of noise-enhanced stability, both under internal (thermal) noise and under externally injected noise, supports the view that controlled fluctuations can become a practical knob for stabilizing operation, improving reproducibility, and shaping switching kinetics in neuromorphic and memory-oriented platforms.

A complementary quantum perspective emerges in driven dissipative bistable systems described within the Caldeira–Leggett framework. There, the escape dynamics from a metastable region exhibits a crossover controlled by system–bath coupling: from a regime where driving frequency produces resonant peaks and dips in the escape time, to a strongly dissipative regime where the escape becomes essentially frequency independent and the dynamics is dominated by dissipation-controlled depletion pathways. This behavior constitutes a quantum analogue of noise-assisted control, showing that dissipation, when properly engineered, can be used to tailor metastable lifetimes rather than merely destroying coherence.

Finally, we discussed an application at the interface of nonlinear dynamics and fundamental physics: axion-induced modifications of Josephson switching statistics. Within the effective coupling hypothesis, scanning the ratio between axion and Josephson energy scales can generate a minimum in the mean switching time, accompanied by a similar modulation of the distribution width. Independently of the broader debate on microscopic coupling mechanisms, this framing suggests a concrete statistical protocol: repeated switching measurements, combined with controlled scans of junction parameters, can be used to search for reproducible, parameter-locked signatures that go beyond a shift of the mean and involve the full switching-time distribution.

Overall, the examples reviewed here show that metastability provides a unifying language across classical, quantum, and device-level settings, and that noise-assisted phenomena can be leveraged both to interpret complex dynamics and to design robust control and sensing strategies.

## Declaration of conflicting interests

The author(s) declared no potential conflicts of interest with respect to the research, authorship, and/or publication of this article.

## Funding

This work was partially supported by Italian Ministry of University and Research (MUR) and National Center for Physics and Mathematics (section No. 9 of scientific program “Artificial intelligence and big data in technical, industrial, natural and social

systems”). D.V. acknowledges support from European Union - Next Generation EU through project THENCE - Partenariato Esteso NQSTI - PE00000023 - Spoke 2.

## References

Agudov N and Spagnolo B (2001) Noise enhanced stability of periodically driven metastable states. *Physical Review E* 64: 035102. DOI:10.1103/PhysRevE.64.035102. URL <https://doi.org/10.1103/PhysRevE.64.035102>. Rapid Communication.

Agudov NV, Dubkov AA and Spagnolo B (2003) Escape from a metastable state with fluctuating barrier. *Physica A: Statistical Mechanics and its Applications* 325(1): 144–151. DOI:[https://doi.org/10.1016/S0378-4371\(03\)00193-6](https://doi.org/10.1016/S0378-4371(03)00193-6). URL <https://www.sciencedirect.com/science/article/pii/S0378437103001936>. Stochastic Systems: From Randomness to Complexity.

Agudov NV, Safonov AV, Krichigin AV, Kharcheva AA, Dubkov AA, Valenti D, Guseinov DV, Belov AI, Mikhaylov AN, Carollo A and Spagnolo B (2020) Nonstationary distributions and relaxation times in a stochastic model of memristor. *Journal of Statistical Mechanics: Theory and Experiment* 2020(2): 024003. DOI:10.1088/1742-5468/ab684a. URL <https://doi.org/10.1088/1742-5468/ab684a>.

Alonso F, Maldonado D, Aguilera A and Roldán J (2021) Memristor variability and stochastic physical properties modeling from a multivariate time series approach. *Chaos, Solitons & Fractals* 143: 110461. DOI: <https://doi.org/10.1016/j.chaos.2020.110461>. URL <https://www.sciencedirect.com/science/article/pii/S0960077920308535>.

Alsuwian T, Kousar F, Rasheed U, Imran M, Hussain F, Arif Khalil R, Algadi H, Batool N, Khera EA, Kiran S and Ashiq MN (2021) First principles investigation of physically conductive bridge filament formation of aluminum doped perovskite materials for neuromorphic memristive applications. *Chaos, Solitons & Fractals* 150: 111111. DOI:<https://doi.org/10.1016/j.chaos.2021.111111>. URL <https://www.sciencedirect.com/science/article/pii/S0960077921004653>.

Asztalos SJ, Carosi G, Hagmann C, Kinion D, van Bibber K, Hotz M, Rosenberg LJ, Rybka G, Hoskins J, Hwang J, Sikivie P, Tanner DB, Bradley R and Clarke J (2010) Squid-based microwave cavity search for dark-matter axions. *Phys. Rev. Lett.* 104: 041301. DOI:10.1103/PhysRevLett.104.041301. URL <https://link.aps.org/doi/10.1103/PhysRevLett.104.041301>.

Barone A and Paterno G (1982) *Physics and applications of the Josephson effect*. Wiley, New York.

Bartram ea (2023) Dark matter axion search using a josephson traveling wave parametric amplifier. *Review of Scientific Instruments* 94(4): 044703. DOI:10.1063/5.0122907. URL <https://doi.org/10.1063/5.0122907>.

Beck C (2011) Testing axion physics in a josephson junction environment. *Modern Physics Letters A* 26(38): 2841–2852.

Beck C (2012) Axion physics in a josephson junction environment. *Physica C: Superconductivity* 473: 21–25.

Beck C (2013) Possible resonance effect of axionic dark matter in josephson junctions. *Phys. Rev. Lett.* 111: 231801.

Beck C (2015) Axion mass estimates from resonant josephson junctions. *Physics of the Dark Universe* 7-8: 6–11.

Beck C (2016) Cosmological flux noise and measured noise power spectra in squids. *Scientific Reports* 6(1): 28275.

Bergeret FS and Cuevas JC (2008) The vortex state and josephson critical current of a diffusive sns junction. *Journal of Low Temperature Physics* 153(5): 304–324.

Bhatia V, Mulgrew B and Georgiadis A (2006) Stochastic gradient algorithms for equalisation in  $\alpha$ -stable noise. *Signal Processing* 86(4): 835 – 845. DOI: <https://doi.org/10.1016/j.sigpro.2005.06.013>. URL <https://www.sciencedirect.com/science/article/pii/S0165168405002380>.

Blackburn JA, Cirillo M and Grønbech-Jensen N (2016) A survey of classical and quantum interpretations of experiments on josephson junctions at very low temperatures. *Physics Reports* 611: 1–33. DOI: <https://doi.org/10.1016/j.physrep.2015.10.010>. URL <https://www.sciencedirect.com/science/article/pii/S0370157315004433>. A survey of classical and quantum interpretations of experiments on Josephson junctions at very low temperatures.

Boldyrev S and Gwinn CR (2003) Lévy model for interstellar scintillations. *Phys. Rev. Lett.* 91: 131101. DOI:10.1103/PhysRevLett.91.131101. URL <https://link.aps.org/doi/10.1103/PhysRevLett.91.131101>.

Boldyrev S and Gwinn CR (2005) Radio-wave propagation in the non-gaussian interstellar medium. *Astrophys. J* 624(1): 213–222. DOI:10.1086/428919. URL <https://doi.org/10.1086%2F428919>.

Boldyrev S and Konigl A (2006) Non-gaussian radio-wave scattering in the interstellar medium. *Astrophys. J* 640(1): 344–352. DOI:10.1086/499219. URL <https://doi.org/10.1086%2F499219>.

Boybat I, Le Gallo M, Nandakumar SR, Moraitsis T, Parnell T, Tuma T, Rajendran B, Leblebici Y, Sebastian A and Eleftheriou E (2018) Neuromorphic computing with multi-memristive synapses. *Nature Communications* 9(1): 2514. DOI:10.1038/s41467-018-04933-y. URL <https://doi.org/10.1038/s41467-018-04933-y>.

Braggio C, Balembois L, Di Vora R, Wang Z, Travedo J, Pallegoix L, Carugno G, Ortolan A, Ruoso G, Gambardella U, D’Agostino D, Bertet P and Flurin E (2025) Quantum-enhanced sensing of axion dark matter with a transmon-based single microwave photon counter.

*Phys. Rev. X* 15: 021031. DOI:10.1103/PhysRevX.15.021031. URL <https://link.aps.org/doi/10.1103/PhysRevX.15.021031>.

Braginski AI (2019) Superconductor electronics: Status and outlook. *Journal of Superconductivity and Novel Magnetism* 32(1): 23–44.

Briskot U, Dmitriev IA and Mirlin AD (2014) Relaxation of optically excited carriers in graphene: Anomalous diffusion and lévy flights. *Phys. Rev. B* 89: 075414. DOI:10.1103/PhysRevB.89.075414. URL <http://link.aps.org/doi/10.1103/PhysRevB.89.075414>.

Brockmann D, Hufnagel L and Geisel T (2006) The scaling laws of human travel. *Nature* 439(7075): 462–465. DOI:10.1038/nature04292. URL <https://doi.org/10.1038/nature04292>.

Brokmann X, Hermier JP, Messin G, Desbiolles P, Bouchaud JP and Dahan M (2003) Statistical aging and nonergodicity in the fluorescence of single nanocrystals. *Phys. Rev. Lett.* 90: 120601. DOI:10.1103/PhysRevLett.90.120601. URL <https://link.aps.org/doi/10.1103/PhysRevLett.90.120601>.

Caldeira AO and Leggett AJ (1983) Path integral approach to quantum brownian motion. *Annals of Physics* 149: 374–456.

Chechkin AV, Gonchar VY, Klafter J and Metzler R (2005) Barrier crossing of a Lévy flight. *Europhysics Letters* 72: 348. DOI: 10.1209/epl/i2005-10265-1. URL <https://doi.org/10.1209/epl/i2005-10265-1>.

Chechkin AV, Sliusarenko OY, Metzler R and Klafter J (2007) Barrier crossing driven by Lévy noise: Universality and the role of noise intensity. *Physical Review E* 75: 041101. DOI: 10.1103/PhysRevE.75.041101. URL <https://doi.org/10.1103/PhysRevE.75.041101>.

Chen YF, Hover D, Sendelbach S, Maurer L, Merkel ST, Pritchett EJ, Wilhelm FK and McDermott R (2011) Microwave photon counter based on josephson junctions. *Phys. Rev. Lett.* 107: 217401. DOI:10.1103/PhysRevLett.107.217401. URL <https://link.aps.org/doi/10.1103/PhysRevLett.107.217401>.

Chouri B, Fabrice M, Dandache A, Aroussi ME and Saadane R (2014) Bearing fault diagnosis based on alpha-stable distribution feature extraction and svm classifier. In: *2014 International Conference on Multimedia Computing and Systems (ICMCS)*. pp. 1545–1550.

Chua L (1971) Memristor-the missing circuit element. *IEEE Transactions on Circuit Theory* 18(5): 507–519. DOI:10.1109/TCT.1971.1083337.

Chua LO, Tetzlaff R and Slavova A (eds.) (2022) *Memristor Computing Systems*. 1 edition. Springer Cham. ISBN 978-3-030-90582-8. DOI:10.1007/978-3-030-90582-8. URL <https://link.springer.com/book/10.1007/978-3-030-90582-8>.

Citro R, Guarcello C and Pagano S (2024) *Josephson Junctions, Superconducting Circuits, and Qubit for Quantum Technologies*. Cham: Springer Nature Switzerland. ISBN 978-3-031-55657-9, pp. 1–59. DOI:10.1007/978-3-031-55657-9\_1. URL [https://doi.org/10.1007/978-3-031-55657-9\\_1](https://doi.org/10.1007/978-3-031-55657-9_1).

Co RT, Hall LJ and Harigaya K (2020) Axion kinetic misalignment mechanism. *Phys. Rev. Lett.* 124: 251802.

Cortes JA, Diez L, Canete FJ and Sanchez-Martinez JJ (2010) Analysis of the indoor broadband power-line noise scenario. *IEEE Transactions on Electromagnetic Compatibility* 52(4): 849–858.

De Simoni G, Paolucci F, Puglia C and Giazotto F (2019) Josephson field-effect transistors based on all-metallic al/cu/al proximity nanojunctions. *ACS Nano* 13(7): 7871–7876.

De Stefano S, Durante O, D’Orsi R, Operamolla A, Ambroco M, Ambroco PF, Martuccello N, Giubileo F and Di Bartolomeo A (2024) Resistive switching memory from dielectric lignin for sustainable electronics. *J. Mater. Chem. C* 12: 13621–13631. DOI:10.1039/D4TC02229G. URL <http://dx.doi.org/10.1039/D4TC02229G>.

Devoret MH, Martinis JM, Esteve D and Clarke J (1984) Resonant activation from the zero-voltage state of a current-biased josephson junction. *Phys. Rev. Lett.* 53: 1260–1263.

Devoret MH and Schoelkopf RJ (2013) Superconducting circuits for quantum information: An outlook. *Science* 339(6124): 1169–1174.

Ditlevsen PD (1999) Observation of  $\alpha$ -stable noise induced millennial climate changes from an ice-core record. *Geophysical Research Letters* 26(10): 1441–1444. DOI:<https://doi.org/10.1029/1999GL900252>. URL <https://agupubs.onlinelibrary.wiley.com/doi/abs/10.1029/1999GL900252>.

Doering CR and Gadoua JC (1992) Resonant activation over a fluctuating barrier. *Phys. Rev. Lett.* 69: 2318–2321.

Du X, Skachko I and Andrei EY (2008) Josephson current and multiple andreev reflections in graphene sns junctions. *Phys. Rev. B* 77: 184507.

Dubkov A and Spagnolo B (2005) Generalized wiener process and kolmogorov’s equation for diffusion induced by non-gaussian noise source. *Fluctuation and Noise Letters* 5: L267. DOI: 10.1142/S0219477505002641. URL <https://doi.org/10.1142/S0219477505002641>.

Dubkov AA, Agudov NV and Spagnolo B (2004) Noise-enhanced stability in fluctuating metastable states. *Physical Review E* 69: 061103. DOI:10.1103/PhysRevE.69.061103. URL <https://doi.org/10.1103/PhysRevE.69.061103>.

Dubkov AA, Dybiec B, Spagnolo B, Kharcheva A, Guarcello C and Valenti D (2020) Statistics of residence time for lévy flights in unstable parabolic potentials. *Phys. Rev. E* 102: 042142. DOI:10.1103/PhysRevE.102.042142.

042142. URL <https://link.aps.org/doi/10.1103/PhysRevE.102.042142>.

Dubkov AA, Guarcello C and Spagnolo B (2025) Enhancement of stability of metastable states in the presence of Lévy noise. *SciPost Phys.* 18: 006. DOI:10.21468/SciPostPhys.18.1.006. URL <https://scipost.org/10.21468/SciPostPhys.18.1.006>.

Dubkov AA, Spagnolo B and Uchaikin VV (2008) Lévy flight superdiffusion: an introduction. *Int. J. Bifurcation Chaos Appl. Sci. Eng.* 18(09): 2649–2672.

Dubos P, Courtois H, Pannetier B, Wilhelm FK, Zaikin AD and Schön G (2001) Josephson critical current in a long mesoscopic s-n-s junction. *Phys. Rev. B* 63: 064502.

Dybiec B, Gudowska-Nowak E and Hänggi P (2007) Escape driven by  $\alpha$ -stable white noises. *Physical Review E* 75: 021109. DOI:10.1103/PhysRevE.75.021109. URL <https://doi.org/10.1103/PhysRevE.75.021109>.

Elyassami Y, Benjelloun K and El Aroussi M (2016) Bearing fault diagnosis and classification based on kda and alpha-stable fusion. *Contemp. Eng. Sci.* 9: 453–465.

Facchi P, Tasaki S, Pascazio S, Nakazato H, Tokuse A and Lidar DA (2005) Control of decoherence: Analysis and comparison of three different strategies. *Phys. Rev. A* 71: 022302. DOI:10.1103/PhysRevA.71.022302. URL <https://link.aps.org/doi/10.1103/PhysRevA.71.022302>.

Feynman RP and Vernon FLJ (1963) The theory of a general quantum system interacting with a linear dissipative system. *Annals of Physics* 24: 118–173.

Fiasconaro A, Spagnolo B and Boccaletti S (2005) Signatures of noise-enhanced stability in metastable states. *Physical Review E* 72: 061110. DOI:10.1103/PhysRevE.72.061110. URL <https://doi.org/10.1103/PhysRevE.72.061110>.

Filatov D, Koryazhkina M, Novikov A, Shishmakova V, Shenina M, Antonov I, Gorshkov O, Agudov N, Carollo A, Valenti D and Spagnolo B (2022) Effect of internal noise on the relaxation time of an yttria stabilized zirconia-based memristor. *Chaos, Solitons & Fractals* 156: 111810. DOI:<https://doi.org/10.1016/j.chaos.2022.111810>. URL <https://www.sciencedirect.com/science/article/pii/S0960077922000212>.

Filatov DO, Vrzheschch DV, Tabakov OV, Novikov AS, Belov AI, Antonov IN, Sharkov VV, Koryazhkina MN, Mikhaylov AN, Gorshkov ON, Dubkov AA, Carollo A and Spagnolo B (2019) Noise-induced resistive switching in a memristor based on zro2(y)/ta2o5 stack. *Journal of Statistical Mechanics: Theory and Experiment* 2019(12): 124026. DOI: 10.1088/1742-5468/ab5704. URL <https://doi.org/10.1088/1742-5468/ab5704>.

Fonseca DB, Barbosa ALR and Pereira LFC (2024) Lévy flight for electrons in graphene in the presence of regions with enhanced spin-orbit coupling. *Phys. Rev. B* 110: 075421. DOI:10.1103/PhysRevB.110.075421. URL <https://link.aps.org/doi/10.1103/PhysRevB.110.075421>.

Fonseca DB, Pereira LFC and Barbosa ALR (2023) Lévy flight for electrons in graphene: Superdiffusive-to-diffusive transport transition. *Phys. Rev. B* 107: 155432. DOI:10.1103/PhysRevB.107.155432. URL <https://link.aps.org/doi/10.1103/PhysRevB.107.155432>.

Frick N, Hosseini M, Guilbaud D, Gao M and LaBean TH (2022) Modeling and characterization of stochastic resistive switching in single ag2s nanowires. *Scientific Reports* 12(1): 6754. DOI:10.1038/s41598-022-09893-4. URL <https://doi.org/10.1038/s41598-022-09893-4>.

Gaba S, Sheridan P, Zhou J, Choi S and Lu W (2013) Stochastic memristive devices for computing and neuromorphic applications. *Nanoscale* 5: 5872–5878. DOI:10.1039/C3NR01176C. URL <http://dx.doi.org/10.1039/C3NR01176C>.

Gattenlöhner S, Gornyi IV, Ostrovsky PM, Trauzettel B, Mirlin AD and Titov M (2016) Lévy flights due to anisotropic disorder in graphene. *Phys. Rev. Lett.* 117: 046603. DOI:10.1103/PhysRevLett.117.046603. URL <https://link.aps.org/doi/10.1103/PhysRevLett.117.046603>.

Gnedenko BV and Kolmogorov AN (1954) *Limit Distributions for Sums of Independent Random Variables*. Cambridge: Addison-Wesley. Ark:/13960/s21dz174pxw.

Grifoni M and Hänggi P (1998) Driven quantum tunneling. *Physics Reports* 304(5): 229–354. DOI: [https://doi.org/10.1016/S0370-1573\(98\)00022-2](https://doi.org/10.1016/S0370-1573(98)00022-2). URL <https://www.sciencedirect.com/science/article/pii/S0370157398000222>.

Grimaudo R, Valenti D, Filatrella G, Spagnolo B and Guarcello C (2023a) Coupled quantum pendula as a possible model for josephson-junction-based axion detection. *Chaos, Solitons & Fractals* 173: 113745. DOI:<https://doi.org/10.1016/j.chaos.2023.113745>. URL <https://www.sciencedirect.com/science/article/pii/S096007792300646X>.

Grimaudo R, Valenti D, Spagnolo B, Filatrella G and Guarcello C (2022) Josephson-junction-based axion detection through resonant activation. *Phys. Rev. D* 105: 033007. DOI:10.1103/PhysRevD.105.033007. URL <https://link.aps.org/doi/10.1103/PhysRevD.105.033007>.

Grimaudo R, Valenti D, Spagnolo B, Troisi A, Filatrella G and Guarcello C (2023b) Axion field influence on josephson junction quasipotential. *Materials* 16(17): 5972. DOI: 10.3390/ma16175972. URL <https://www.mdpi.com/1996-1944/16/17/5972>.

Guarcello C (2021) Lévy noise effects on josephson junctions. *Chaos, Solitons & Fractals* 153: 111531. DOI:<https://doi.org/10.1016/j.chaos.2021.111531>. URL <https://www.sciencedirect.com/science/article/pii/S0960077921008857>.

Guarcello C and Bergeret F (2021) Thermal noise effects on the magnetization switching of a ferromagnetic anomalous josephson junction. *Chaos, Solitons & Fractals* 142: 110384. DOI:<https://doi.org/10.1016/j.chaos.2020.110384>. URL <https://www.sciencedirect.com/science/article/pii/S0960077920307785>.

Guarcello C, Bergeret FS and Citro R (2023) Switching current distributions in ferromagnetic anomalous josephson junctions. *Applied Physics Letters* 123(15): 152602. DOI:10.1063/5.0167769. URL <https://doi.org/10.1063/5.0167769>.

Guarcello C, Filatrella G, De Santis D, Spagnolo B and Valenti D (2024a) Lévy noise-induced effects in a long josephson junction in the presence of two different spatial noise distributions. *Chaos, Solitons & Fractals* 187: 115421. DOI:<https://doi.org/10.1016/j.chaos.2024.115421>. URL <https://www.sciencedirect.com/science/article/pii/S0960077924009731>.

Guarcello C, Filatrella G, Spagnolo B, Pierro V and Valenti D (2020) Voltage drop across josephson junctions for lévy noise detection. *Phys. Rev. Research* 2: 043332. DOI:10.1103/PhysRevResearch.2.043332. URL <https://link.aps.org/doi/10.1103/PhysRevResearch.2.043332>.

Guarcello C, Giazotto F and Solinas P (2016) Coherent diffraction of thermal currents in long josephson tunnel junctions. *Phys. Rev. B* 94: 054522. DOI:10.1103/PhysRevB.94.054522.

Guarcello C, Pagano S and Filatrella G (2024b) Efficiency of diode effect in asymmetric inline long Josephson junctions. *Applied Physics Letters* 124(16): 162601. DOI:10.1063/5.0211230. URL <https://doi.org/10.1063/5.0211230>.

Guarcello C, Piedjou Komnang AS, Barone C, Rettaroli A, Gatti C, Pagano S and Filatrella G (2021) Josephson-based scheme for the detection of microwave photons. *Phys. Rev. Applied* 16: 054015.

Guarcello C, Solinas P, Di Ventra M and Giazotto F (2017a) Solitonic josephson-based meminductive systems. *Scientific Reports* 7(1): 46736. DOI:10.1038/srep46736. URL <https://doi.org/10.1038/srep46736>.

Guarcello C, Valenti D and Spagnolo B (2015) Phase dynamics in graphene-based josephson junctions in the presence of thermal and correlated fluctuations. *Phys. Rev. B* 92: 174519.

Guarcello C, Valenti D, Spagnolo B, Pierro V and Filatrella G (2017b) Anomalous transport effects on switching currents of graphene-based josephson junctions. *Nanotechnology* 28(13): 134001.

Guarcello C, Valenti D, Spagnolo B, Pierro V and Filatrella G (2019) Josephson-based threshold detector for lévy-distributed current fluctuations. *Phys. Rev. Applied* 11: 044078. DOI:10.1103/PhysRevApplied.11.044078. URL <https://link.aps.org/doi/10.1103/PhysRevApplied.11.044078>.

Guo T, Pan K, Jiao Y, Sun B, Du C, Mills JP, Chen Z, Zhao X, Wei L, Zhou YN and Wu YA (2022) Versatile memristor for memory and neuromorphic computing. *Nanoscale Horiz.* 7: 299–310. DOI:10.1039/D1NH00481F. URL <http://dx.doi.org/10.1039/D1NH00481F>.

Gwinn CR (2007) Observations and levy statistics in interstellar scattering. *Astron. Astrophys. Trans.* 26(6): 525–533. DOI:10.1080/10556790701610506. URL <https://doi.org/10.1080/10556790701610506>.

Harris DO, Engerholm GG and Gwinn WD (1965) Calculation of matrix elements for one-dimensional quantum-mechanical problems and the application to anharmonic oscillators. *The Journal of Chemical Physics* 43(5): 1515–1517. DOI:10.1063/1.1696963. URL <https://doi.org/10.1063/1.1696963>.

Huang W, Xia X, Zhu C, Steichen P, Quan W, Mao W, Yang J, Chu L and Li X (2021) Memristive artificial synapses for neuromorphic computing. *Nano-Micro Letters* 13(1): 85. DOI:10.1007/s40820-021-00618-2. URL <https://doi.org/10.1007/s40820-021-00618-2>.

Hurtado PI, Marro J and Garrido PL (2006) Metastability, nucleation, and noise-enhanced stabilization out of equilibrium. *Physical Review E* 74: 050101. DOI:10.1103/PhysRevE.74.050101. URL <https://doi.org/10.1103/PhysRevE.74.050101>. Rapid Communication.

Hussain F, Imran M, Khalil RA, Sattar MA, Niaz NA, Rana AM, Ismail M, Khera EA, Rasheed U, Mumtaz F, Javed T and Kim S (2019) A first-principles study of cu and al doping in zro2 for rram device applications. *Vacuum* 168: 108842. DOI:<https://doi.org/10.1016/j.vacuum.2019.108842>. URL <https://www.sciencedirect.com/science/article/pii/S0042207X19312102>.

Ielmini D and Waser R (2016) *Resistive Switching: From Fundamentals of Nanoionic Redox Processes to Memristive Device Applications*. Saarbrücken: Wiley-VCH. ISBN 9783527680870. DOI:10.1002/9783527680870. URL <https://onlinelibrary.wiley.com/doi/book/10.1002/9783527680870>.

Imkeller P, Pavlyukevich I and Wetzel T (2009) First exit times for Lévy-driven diffusions with exponentially light jumps. *The Annals of Probability* 37: 530. DOI:10.1214/08-AOP412. URL <https://doi.org/10.1214/08-AOP412>.

Imkeller P, Pavlyukevich I and Wetzel T (2010) The hierarchy of exit times of Lévy-driven langevin equations. *The European Physical Journal Special Topics* 191: 211. DOI:10.1140/epjst/e2010-01351-7. URL <https://doi.org/10.1140/epjst/e2010-01351-7>.

Irastorza IG and Redondo J (2018) New experimental approaches in the search for axion-like particles. *Progress in Particle and Nuclear Physics* 102: 89–159.

Jespersen S, Metzler R and Fogedby HC (1999) Lévy flights in external force fields: Langevin and fractional fokker-planck

equations and their solutions. *Physical Review E* 59: 2736. DOI:10.1103/PhysRevE.59.2736. URL <https://doi.org/10.1103/PhysRevE.59.2736>.

Karakus O, Kuruoglu EE and Altinkaya MA (2020) Modelling impulsive noise in indoor powerline communication systems. *Signal, Image and Video Processing* 14(8): 1655–1661. DOI: 10.1007/s11760-020-01708-1. URL <https://doi.org/10.1007/s11760-020-01708-1>.

Kautz RL (1996) Noise, chaos, and the josephson voltage standard. *Reports on Progress in Physics* 59(8): 935–992.

Khan R, Ilyas N, Shamim MZM, Khan MI, Sohail M, Rahman N, Khan AA, Khan SN and Khan A (2021) Oxide-based resistive switching-based devices: fabrication, influence parameters and applications. *J. Mater. Chem. C* 9: 15755–15788. DOI:10.1039/D1TC03420K. URL <http://dx.doi.org/10.1039/D1TC03420K>.

Khera EA, Mahata C, Imran M, Niaz NA, Hussain F, Khalil RMA, Rasheed U and SungjunKim (2022) Improved resistive switching characteristics of a multi-stacked hfo<sub>2</sub>/al<sub>2</sub>o<sub>3</sub>/hfo<sub>2</sub> rram structure for neuromorphic and synaptic applications: experimental and computational study. *RSC Adv.* 12: 11649–11656. DOI:10.1039/D1RA08103A. URL <http://dx.doi.org/10.1039/D1RA08103A>.

Kim HD, Yun M and Kim S (2015) Self-rectifying resistive switching behavior observed in si3n4-based resistive random access memory devices. *Journal of Alloys and Compounds* 651: 340–343. DOI:<https://doi.org/10.1016/j.jallcom.2015.08.082>. URL <https://www.sciencedirect.com/science/article/pii/S0925838815307787>.

Kiselev EI and Schmalian J (2019) Lévy flights and hydrodynamic superdiffusion on the dirac cone of graphene. *Phys. Rev. Lett.* 123: 195302. DOI:10.1103/PhysRevLett.123.195302. URL <https://link.aps.org/doi/10.1103/PhysRevLett.123.195302>.

Kjaergaard M, Schwartz ME, Braumüller J, Krantz P, Wang JIJ, Gustavsson S and Oliver WD (2020) Superconducting qubits: Current state of play. *Annual Review of Condensed Matter Physics* 11(1): 369–395.

Koryazhina M, Filatov D, Shishmakova V, Shenina M, Belov A, Antonov I, Kotomina V, Mikhaylov A, Gorshkov O, Agudov N, Guarcello C, Carollo A and Spagnolo B (2022) Resistive state relaxation time in zro<sub>2</sub>(y)-based memristive devices under the influence of external noise. *Chaos, Solitons & Fractals* 162: 112459. DOI:<https://doi.org/10.1016/j.chaos.2022.112459>. URL <https://www.sciencedirect.com/science/article/pii/S0960077922006695>.

Kousar F, Rasheed U, Khalil RMA, Niaz NA, Hussain F, Imran M, Shakoor U, Algadi H and Ashiq N (2021) First principles investigation of oxygen vacancies filaments in polymorphic titania and their role in memristor's applications. *Chaos, Solitons & Fractals* 148: 111024. DOI:<https://doi.org/10.1016/j.chaos.2021.111024>. URL <https://www.sciencedirect.com/science/article/pii/S0960077921003787>.

Kramers HA (1940) Brownian motion in a field of force and the diffusion model of chemical reactions. *Physica* 7: 284. DOI: 10.1016/S0031-8914(40)90098-2. URL [https://doi.org/10.1016/S0031-8914\(40\)90098-2](https://doi.org/10.1016/S0031-8914(40)90098-2).

Krantz P, Kjaergaard M, Yan F, Orlando TP, Gustavsson S and Oliver WD (2019) A quantum engineer's guide to superconducting qubits. *Applied Physics Reviews* 6: 021318.

Kuno M, Fromm DP, Hamann HF, Gallagher A and Nesbitt DJ (2000) Nonexponential "blinking" kinetics of single cdse quantum dots: A universal power law behavior. *J. Chem. Phys.* 112(7): 3117–3120. DOI:10.1063/1.480896. URL <https://doi.org/10.1063/1.480896>.

Kuno M, Fromm DP, Hamann HF, Gallagher A and Nesbitt DJ (2001) "on"/"off" fluorescence intermittency of single semiconductor quantum dots. *J. Chem. Phys.* 115(2): 1028–1040. DOI:10.1063/1.1377883. URL <https://doi.org/10.1063/1.1377883>.

Kuzmin LS, Sobolev AS, Gatti C, Di Gioacchino D, Crescini N, Gordeeva A and Il'ichev E (2018) Single photon counter based on a josephson junction at 14 ghz for searching galactic axions. *IEEE Transactions on Applied Superconductivity* 28(7): 1–5. DOI:10.1109/TASC.2018.2850019.

Ladeynov D, Egorov D and Pankratov A (2023) Stochastic versus dynamic resonant activation to enhance threshold detector sensitivity. *Chaos, Solitons & Fractals* 171: 113506. DOI:<https://doi.org/10.1016/j.chaos.2023.113506>. URL <https://www.sciencedirect.com/science/article/pii/S0960077923004071>.

Lee GH, Efetov DK, Jung W, Ranzani L, Walsh ED, Ohki TA, Taniguchi T, Watanabe K, Kim P, Englund D and Fong KC (2020) Graphene-based josephson junction microwave bolometer. *Nature* 586(7827): 42–46. DOI:10.1038/s41586-020-2752-4.

Lee JS, Lee S and Noh TW (2015) Resistive switching phenomena: A review of statistical physics approaches. *Applied Physics Reviews* 2(3): 031303. DOI:10.1063/1.4929512. URL <https://doi.org/10.1063/1.4929512>.

Lévy P (1937) *Théorie de l'addition des variables Aléatoires*. Paris: Gauthier–Villars. WorldCat-Online Computer Library Center (OCLC): 490351581.

Li C and Yu G (2010) A new statistical model for rolling element bearing fault signals based on alpha-stable distribution. In: *2010 Second International Conference on Computer Modeling and Simulation*, volume 4. pp. 386–390. DOI: 10.1109/ICCMS.2010.309.

Li Y, Wang Z, Midya R, Xia Q and Yang JJ (2018) Review of memristor devices in neuromorphic computing: materials sciences and device challenges. *Journal of Physics D: Applied Physics* 51(50): 503002. DOI:10.1088/1361-6463/aade3f. URL <https://doi.org/10.1088/1361-6463/aade3f>.

1361–6463/aade3f.

Light JC and Carrington T (2007) Discrete-variable representations and their utilization. In: *Advances in Chemical Physics*, volume 114. New York: Wiley, pp. 263–310.

Luryi S and Subashiev A (2010) *Semiconductor Scintillator for Three-Dimensional Array of Radiation Detectors*. John Wiley & Sons, Inc. ISBN 9780470649343, pp. 331–346. DOI: 10.1002/9780470649343.ch28. URL <http://dx.doi.org/10.1002/9780470649343.ch28>.

Lv Z, Wang Y, Chen J, Wang J, Zhou Y and Han ST (2020) Semiconductor quantum dots for memories and neuromorphic computing systems. *Chemical Reviews* 120(9): 3941–4006. DOI:10.1021/acs.chemrev.9b00730. URL <https://doi.org/10.1021/acs.chemrev.9b00730>.

Lv Z, Zhou Y, Han ST and Roy V (2018) From biomaterial-based data storage to bio-inspired artificial synapse. *Materials Today* 21(5): 537–552. DOI: <https://doi.org/10.1016/j.mattod.2017.12.001>. URL <https://www.sciencedirect.com/science/article/pii/S1369702117305977>.

Magazzù L (2015) *Ph.D. thesis*. PhD Thesis, Palermo University, Palermo.

Mahata C, Lee C, An Y, Kim MH, Bang S, Kim CS, Ryu JH, Kim S, Kim H and Park BG (2020) Resistive switching and synaptic behaviors of an hfo<sub>2</sub>/al<sub>2</sub>o<sub>3</sub> stack on ito for neuromorphic systems. *Journal of Alloys and Compounds* 826: 154434. DOI:<https://doi.org/10.1016/j.jallcom.2020.154434>. URL <https://www.sciencedirect.com/science/article/pii/S0925838820307970>.

Mantegna RN and Stanley HE (1995) Scaling behaviour in the dynamics of an economic index. *Nature* 376(6535): 46–49. DOI:10.1038/376046a0. URL <https://doi.org/10.1038/376046a0>.

McCumber DE (1968) Effect of ac Impedance on dc Voltage-Current Characteristics of Superconductor Weak-Link Junctions. *Journal of Applied Physics* 39(7): 3113–3118. DOI:10.1063/1.1656743. URL <https://doi.org/10.1063/1.1656743>.

McFadden P and Smith J (1984) Model for the vibration produced by a single point defect in a rolling element bearing. *Journal of Sound and Vibration* 96(1): 69 – 82. DOI:[https://doi.org/10.1016/0022-460X\(84\)90595-9](https://doi.org/10.1016/0022-460X(84)90595-9). URL <https://www.sciencedirect.com/science/article/pii/0022460X84905959>.

Messin G, Hermier JP, Giacobino E, Desbiolles P and Dahan M (2001) Bunching and antibunching in the fluorescence of semiconductor nanocrystals. *Opt. Lett.* 26(23): 1891–1893. DOI:10.1364/OL.26.001891. URL <http://ol.osa.org/abstract.cfm?URI=ol-26-23-1891>.

Metzler R and Klafter J (2000) The random walk's guide to anomalous diffusion: a fractional dynamics approach. *Physics Reports* 339: 1–77. DOI: 10.1016/S0370-1573(00)00070-3. URL [https://doi.org/10.1016/S0370-1573\(00\)00070-3](https://doi.org/10.1016/S0370-1573(00)00070-3).

Mikhaylov A, Guseinov D, Belov A, Korolev D, Shishmakova V, Koryazhkina M, Filatov D, Gorshkov O, Maldonado D, Alonso F, Roldán J, Krichigin A, Agudov N, Dubkov A, Carollo A and Spagnolo B (2021) Stochastic resonance in a metal-oxide memristive device. *Chaos, Solitons & Fractals* 144: 110723. DOI:<https://doi.org/10.1016/j.chaos.2021.110723>. URL <https://www.sciencedirect.com/science/article/pii/S096007792100076X>.

Mikhaylov A, Pimashkin A, Pigareva Y, Gerasimova S, Gryaznov E, Shchanikov S, Zuev A, Talanov M, Lavrov I, Demin V, Erokhin V, Lobov S, Mukhina I, Kazantsev V, Wu H and Spagnolo B (2020) Neurohybrid memristive cmos-integrated systems for biosensors and neuroprosthetics. *Frontiers in Neuroscience* Volume 14 - 2020. DOI: 10.3389/fnins.2020.00358. URL <https://www.frontiersin.org/journals/neuroscience/articles/10.3389/fnins.2020.00358>.

Mohammed AMS, Koh YR, Vermeersch B, Lu H, Burke PG, Gossard AC and Shakouri A (2015) Fractal lévy heat transport in nanoparticle embedded semiconductor alloys. *Nano Letters* 15(7): 4269–4273. DOI:10.1021/nl5044665. URL <https://doi.org/10.1021/nl504466511>.

Naous R, Al-Shedivat M, Neftci E, Cauwenberghs G and Salama KN (2016) Stochastic synaptic plasticity with memristor crossbar arrays. In: *2016 IEEE International Symposium on Circuits and Systems (ISCAS)*. pp. 2078–2081. DOI: 10.1109/ISCAS.2016.7538988.

Naous R, Siemon A, Schulten M, Alahmadi H, Kindsmüller A, Lübben M, Heittmann A, Waser R, Salama KN and Menzel S (2021) Theory and experimental verification of configurable computing with stochastic memristors. *Scientific Reports* 11(1): 4218. DOI:10.1038/s41598-021-83382-y. URL <https://doi.org/10.1038/s41598-021-83382-y>.

Nogueira FS, Nussinov Z and van den Brink J (2016) Josephson currents induced by the witten effect. *Phys. Rev. Lett.* 117: 167002.

Novikov DS, Drndic M, Levitov LS, Kastner MA, Jarosz MV and Bawendi MG (2005) Lévy statistics and anomalous transport in quantum-dot arrays. *Phys. Rev. B* 72: 075309. DOI: 10.1103/PhysRevB.72.075309. URL <http://link.aps.org/doi/10.1103/PhysRevB.72.075309>.

Ntinas V, Rubio A, Sirakoulis GC, Aguilera ES, Pedro M, Crespo-Yepes A, Martin-Martinez J, Rodriguez R and Nafria M (2021) Power-efficient noise-induced reduction of reram cell's temporal variability effects. *IEEE Transactions on Circuits and Systems II: Express Briefs* 68(4): 1378–1382. DOI:10.1109/TCSII.2020.3026950.

Ntinas V, Rubio A, Sirakoulis GC, Rodríguez R and Nafría M (2019) Experimental investigation of memristance enhancement. In: *2019 IEEE/ACM International Symposium on Nanoscale Architectures (NANOARCH)*. pp. 1–2. DOI:10.1109/NANOARCH47378.2019.181299.

Oelsner G, Andersen CK, Rehák M, Schmelz M, Anders S, Grajcar M, Hübner U, Mølmer K and Il'ichev E (2017) Detection of weak microwave fields with an underdamped josephson junction. *Phys. Rev. Appl.* 7: 014012. DOI:10.1103/PhysRevApplied.7.014012. URL <https://link.aps.org/doi/10.1103/PhysRevApplied.7.014012>.

Pankratov AL, Gordeeva AV, Chiginev AV, Revin LS, Blagodatkin AV, Crescini N and Kuzmin LS (2025) Detection of single-mode thermal microwave photons using an underdamped josephson junction. *Nature Communications* 16(1): 3457. DOI:10.1038/s41467-025-56040-4. URL <https://doi.org/10.1038/s41467-025-56040-4>.

Pankratov AL, Revin LS, Gordeeva AV, Yablokov AA, Kuzmin LS and Il'ichev E (2022) Towards a microwave single-photon counter for searching axions. *npj Quantum Information* 8(1): 61. DOI:10.1038/s41534-022-00569-5. URL <https://doi.org/10.1038/s41534-022-00569-5>.

Patterson GA, Fierens PI and Grosz DF (2013) On the beneficial role of noise in resistive switching. *Applied Physics Letters* 103(7): 074102. DOI:10.1063/1.4819018. URL <https://doi.org/10.1063/1.4819018>.

Pi S, Li C, Jiang H, Xia W, Xin H, Yang JJ and Xia Q (2019) Memristor crossbar arrays with 6-nm half-pitch and 2-nm critical dimension. *Nature Nanotechnology* 14(1): 35–39. DOI:10.1038/s41565-018-0302-0. URL <https://doi.org/10.1038/s41565-018-0302-0>.

Piedjou Komnang A, Guarcello C, Barone C, Gatti C, Pagano S, Pierro V, Rettaroli A and Filatrella G (2021) Analysis of josephson junctions switching time distributions for the detection of single microwave photons. *Chaos Solitons Fract* 142: 110496.

Rasheed U, Ryu H, Mahata C, Khalil RMA, Imran M, Rana AM, Kousar F, Kim B, Kim Y, Cho S, Hussain F and Kim S (2021) Resistive switching characteristics and theoretical simulation of a pt/a-ta2o5/tin synaptic device for neuromorphic applications. *Journal of Alloys and Compounds* 877: 160204. DOI:<https://doi.org/10.1016/j.jallcom.2021.160204>. URL <https://www.sciencedirect.com/science/article/pii/S0925838821016133>.

Resheed U, Alsuwian T, Imran M, Algadi H, Khera EA, Khalil RMA, Mahata C and Hussain F (2021) Density functional theory insight into metal ions and vacancies for improved performance in storage devices. *International Journal of Energy Research* 45(7): 10882–10894. DOI:<https://doi.org/10.1002/er.6572>. URL <https://onlinelibrary.wiley.com/doi/abs/10.1002/er.6572>.

Rettaroli A, Alesini D, Babusci D, Barone C, Buonomo B, Beretta MM, Castellano G, Chiarello F, Di Gioacchino D, Felici G, Filatrella G, Foggetta LG, Gallo A, Gatti C, Ligi C, Maccarrone G, Mattioli F, Pagano S, Tocci S and Torrioli G (2021) Josephson junctions as single microwave photon counters: Simulation and characterization. *Instruments* 5(3): 022915.

Revin LS, Pankratov AL, Gordeeva AV, Yablokov AA, Rakut IV, Zbrozhek VO and Kuzmin LS (2020) Microwave photon detection by an al josephson junction. *Beilstein Journal of Nanotechnology* 11: 960–965. DOI:<https://doi.org/10.3762/bjnano.11.80>. URL <https://www.sciencedirect.com/science/article/pii/S2190428620000763>.

Reynolds AM (2009) Scale-free animal movement patterns: Lévy walks outperform fractional brownian motions and fractional lévy motions in random search scenarios. *Journal of Physics A: Mathematical and Theoretical* 42(43): 434006. DOI:10.1088/1751-8113/42/43/434006. URL <https://doi.org/10.1088/1751-8113/42/43/434006>.

Saadane R, Aroussi ME and Wahbi M (2015) Wind turbine fault diagnosis method based on *alpha* stable distribution and wieghthed support vector machines. In: *2015 3rd International Renewable and Sustainable Energy Conference (IRSEC)*. pp. 1–5. DOI:10.1109/IRSEC.2015.7455101.

Sargsyan VV, Palchikov YV, Kanokov Z, Adamian GG and Antonenko NV (2007) Coordinate-dependent diffusion coefficients: Decay rate in open quantum systems. *Phys. Rev. A* 75: 062115. DOI:10.1103/PhysRevA.75.062115. URL <https://link.aps.org/doi/10.1103/PhysRevA.75.062115>.

Semyonov O, Subashiev AV, Chen Z and Luryi S (2012) Photon assisted lévy flights of minority carriers in n-inp. *J. Lumin.* 132(8): 1935 – 1943. DOI: <http://dx.doi.org/10.1016/j.jlumin.2012.03.035>. URL <https://www.sciencedirect.com/science/article/pii/S0022231312001688>.

Shi T, Wang R, Wu Z, Sun Y, An J and Liu Q (2021) A review of resistive switching devices: Performance improvement, characterization, and applications. *Small Structures* 2(4): 2000109. DOI:<https://doi.org/10.1002/sstr.202000109>. URL <https://onlinelibrary.wiley.com/doi/abs/10.1002/sstr.202000109>.

Shimizu KT, Neuhauser RG, Leatherdale CA, Empedocles SA, Woo WK and Bawendi MG (2001) Blinking statistics in single semiconductor nanocrystal quantum dots. *Phys. Rev. B* 63: 205316. DOI:10.1103/PhysRevB.63.205316. URL <https://link.aps.org/doi/10.1103/PhysRevB.63.205316>.

Shlesinger MF, Zaslavsky GM and Frisch U (eds.) (1995) *Lévy Flights and Related Topics in Physics, Lecture Notes in Physics*, volume 450. Berlin, Heidelberg: Springer. ISBN 978-3-662-14048-2. DOI:10.1007/3-540-59222-9. Proceedings of the International Workshop Held at Nice, France, 27–30 June 1994.

Shongwe T, Ferreira HC and Han Vinck AJ (2015) *Broadband and Narrow-Band Noise Modeling in Powerline Communications*. John Wiley & Sons, Inc. ISBN 9780471346081. DOI:10.1002/047134608X.W8289. URL <http://dx.doi.org/10.1002/047134608X.W8289>.

Sikivie P (1983) Experimental tests of the "invisible" axion. *Phys. Rev. Lett.* 51: 1415–1417.

Sims DW, Southall EJ, Humphries NE, Hays GC, Bradshaw CJA, Pitchford JW, James A, Ahmed MZ, Brierley AS, Hindell MA, Morritt D, Musyl MK, Righton D, Shepard ELC, Wearmouth VJ, Wilson RP, Witt MJ and Metcalfe JD (2008) Scaling laws of marine predator search behaviour. *Nature* 451(7182): 1098–1102. DOI:10.1038/nature06518. URL <https://doi.org/10.1038/nature06518>.

Stewart WC (1968) Current-voltage characteristics of Josephson junctions. *Applied Physics Letters* 12(8): 277–280. DOI:10.1063/1.1651991. URL <https://doi.org/10.1063/1.1651991>.

Stotland A and Di Ventra M (2012) Stochastic memory: Memory enhancement due to noise. *Phys. Rev. E* 85: 011116. DOI:10.1103/PhysRevE.85.011116. URL <https://link.aps.org/doi/10.1103/PhysRevE.85.011116>.

Strukov DB, Snider GS, Stewart DR and Williams RS (2008) The missing memristor found. *Nature* 453(7191): 80–83. DOI:10.1038/nature06932. URL <https://doi.org/10.1038/nature06932>.

Subashiev AV, Semyonov O, Chen Z and Luryi S (2014) Temperature controlled lévy flights of minority carriers in photoexcited bulk n-inp. *Phys. Lett. A* 378(3): 266 – 269. DOI:<http://dx.doi.org/10.1016/j.physleta.2013.11.007>. URL <http://www.sciencedirect.com/science/article/pii/S0375960113010566>.

Subramanian A, Sundaresan A and Varshney PK (2015) Detection of dependent heavy-tailed signals. *IEEE Transactions on Signal Processing* 63(11): 2790–2803.

Sun W, Gao B, Chi M, Xia Q, Yang JJ, Qian H and Wu H (2019) Understanding memristive switching via in situ characterization and device modeling. *Nature Communications* 10(1): 3453. DOI:10.1038/s41467-019-11411-6. URL <https://doi.org/10.1038/s41467-019-11411-6>.

Sushkov AO (2023) Quantum science and the search for axion dark matter. *PRX Quantum* 4: 020101. DOI:10.1103/PRXQuantum.4.020101. URL <https://link.aps.org/doi/10.1103/PRXQuantum.4.020101>.

Tafuri F (2019) *Fundamentals and Frontiers of the Josephson Effect*, volume 286. Springer, Cham, Switzerland.

Thorwart M, Grifoni M and Hänggi P (2000) Strong coupling theory for driven tunneling and vibrational relaxation. *Phys. Rev. Lett.* 85: 860–863. DOI:10.1103/PhysRevLett.85.860. URL <https://link.aps.org/doi/10.1103/PhysRevLett.85.860>.

Thorwart M, Grifoni M and Hänggi P (2001) Strong coupling theory for tunneling and vibrational relaxation in driven bistable systems. *Annals of Physics* 293(1): 15–66. DOI:<https://doi.org/10.1006/aphy.2001.6174>. URL <https://www.sciencedirect.com/science/article/pii/S0003491601961743>.

Tsihrintzis GA and Nikias CL (1995) Performance of optimum and suboptimum receivers in the presence of impulsive noise modeled as an alpha-stable process. *IEEE Transactions on Communications* 43(2/3/4): 904–914. DOI:10.1109/26.380123.

Upadhyaya M and Aksamija Z (2016) Nondiffusive lattice thermal transport in si-ge alloy nanowires. *Phys. Rev. B* 94: 174303. DOI:10.1103/PhysRevB.94.174303. URL <https://link.aps.org/doi/10.1103/PhysRevB.94.174303>.

Valenti D, Carollo A and Spagnolo B (2018) Stabilizing effect of driving and dissipation on quantum metastable states. *Phys. Rev. A* 97: 042109. DOI:10.1103/PhysRevA.97.042109. URL <https://link.aps.org/doi/10.1103/PhysRevA.97.042109>.

Valenti D, Magazzù L, Caldara P and Spagnolo B (2015) Stabilization of quantum metastable states by dissipation. *Phys. Rev. B* 91: 235412. DOI:10.1103/PhysRevB.91.235412. URL <https://link.aps.org/doi/10.1103/PhysRevB.91.235412>.

Vermeersch B, Carrete J, Mingo N and Shakouri A (2015a) Superdiffusive heat conduction in semiconductor alloys. i. theoretical foundations. *Phys. Rev. B* 91: 085202. DOI:10.1103/PhysRevB.91.085202. URL <https://link.aps.org/doi/10.1103/PhysRevB.91.085202>.

Vermeersch B, Mohammed AMS, Pernot G, Koh YR and Shakouri A (2015b) Superdiffusive heat conduction in semiconductor alloys. ii. truncated lévy formalism for experimental analysis. *Phys. Rev. B* 91: 085203. DOI:10.1103/PhysRevB.91.085203. URL <https://link.aps.org/doi/10.1103/PhysRevB.91.085203>.

Walsh ED, Jung W, Lee GH, Efetov DK, Wu BI, Huang KF, Ohki TA, Taniguchi T, Watanabe K, Kim P, Englund D and Fong KC (2021) Josephson junction infrared single-photon detector. *Science* 372(6540): 409–412.

Wang H, Hu L and Han W (2021a) Resistive switching behavior, mechanism and synaptic characteristics in tio2 nanosheets grown on ti plate by hydrothermal method. *Journal of Alloys and Compounds* 854: 157200. DOI: <https://doi.org/10.1016/j.jallcom.2020.157200>. URL <https://www.sciencedirect.com/science/article/pii/S0925838820335647>.

Wang W, Wang M, Ambrosi E, Bricalli A, Laudato M, Sun Z, Chen X and Ielmini D (2019) Surface diffusion-limited lifetime of silver and copper nanofilaments in resistive switching devices. *Nature Communications* 10(1): 81. DOI:10.1038/s41467-018-07979-0. URL <https://doi.org/10.1038/s41467-018-07979-0>.

10.1038/s41467-018-07979-0.

Wang Y, Gong Y, Huang S, Xing X, Lv Z, Wang J, Yang JQ, Zhang G, Zhou Y and Han ST (2021b) Memristor-based biomimetic compound eye for real-time collision detection. *Nature Communications* 12(1): 5979. DOI: 10.1038/s41467-021-26314-8. URL <https://doi.org/10.1038/s41467-021-26314-8>.

Wang Y, Gong Y, Yang L, Xiong Z, Lv Z, Xing X, Zhou Y, Zhang B, Su C, Liao Q and Han ST (2021c) Mxene-zno memristor for multimodal in-sensor computing. *Advanced Functional Materials* 31(21): 2100144. DOI:<https://doi.org/10.1002/adfm.202100144>. URL <https://advanced.onlinelibrary.wiley.com/doi/abs/10.1002/adfm.202100144>.

Wang Z, Xiao W, Yang H, Zhang S, Zhang Y, Sun K, Wang T, Fu Y, Wang Q, Zhang J, Hasegawa T and He D (2022) Resistive switching memristor: On the direct observation of physical nature of parameter variability. *ACS Applied Materials & Interfaces* 14(1): 1557–1567. DOI:10.1021/acsami.1c19364. URL <https://doi.org/10.1021/acsami.1c19364>.

Weiss U (2012) *Quantum Dissipative Systems*. G - Reference,Information and Interdisciplinary Subjects Series. World Scientific. ISBN 9789814374910. URL <https://books.google.it/books?id=qgfuFZxvGKQC>.

West BJ and Deering W (1994) Fractal physiology for physicists: Lévy statistics. *Physics Reports* 246(1): 1–100. DOI: [https://doi.org/10.1016/0370-1573\(94\)00055-7](https://doi.org/10.1016/0370-1573(94)00055-7). URL <https://www.sciencedirect.com/science/article/pii/0370157394000557>.

West BJ, Grigolini P, Metzler R and Nonnenmacher TF (1997) Fractional diffusion and Lévy stable processes. *Physical Review E* 55: 99. DOI:10.1103/PhysRevE.55.99. URL <https://doi.org/10.1103/PhysRevE.55.99>.

White M (1984) Simulation and analysis of machinery fault signals. *Journal of Sound and Vibration* 93(1): 95 – 116. DOI:[https://doi.org/10.1016/0022-460X\(84\)90353-5](https://doi.org/10.1016/0022-460X(84)90353-5). URL <http://www.sciencedirect.com/science/article/pii/0022460X84903535>.

Wu H, Li X, Wu M, Huang F, Yu Z and Qian H (2014) Resistive switching performance improvement of  $\text{ta}_{205-x}/\text{ta}_y$  bilayer reram devices by inserting  $\text{al}_\delta$  barrier layer. *IEEE Electron Device Letters* 35(1): 39–41. DOI: 10.1109/LED.2013.2288311.

Yang JJ, Strukov DB and Stewart DR (2013) Memristive devices for computing. *Nature Nanotechnology* 8(1): 13–24. DOI: 10.1038/nnano.2012.240. URL <https://doi.org/10.1038/nnano.2012.240>.

Yang X and Petropulu AP (2003) Co-channel interference modeling and analysis in a poisson field of interferers in wireless communications. *IEEE Transactions on Signal Processing* 51(1): 64–76. DOI:10.1109/TSP.2002.806591.

Yanovsky VV, Chechkin AV, Schertzer D and Tur AV (2000) Lévy anomalous diffusion and fractional fokker-planck equation. *Physica A* 282: 13. DOI:10.1016/S0378-4371(99)00565-8. URL [https://doi.org/10.1016/S0378-4371\(99\)00565-8](https://doi.org/10.1016/S0378-4371(99)00565-8).

Yu S (2016) *Resistive Random Access Memory (RRAM)*. Synthesis Lectures on Emerging Engineering Technologies, 1 edition. Springer Cham. ISBN 978-3-031-02030-8. DOI:10.1007/978-3-031-02030-8. URL <https://link.springer.com/book/10.1007/978-3-031-02030-8>.

Yu S, Chen HY, Gao B, Kang J and Wong HSP (2013) Hfox-based vertical resistive switching random access memory suitable for bit-cost-effective three-dimensional cross-point architecture. *ACS Nano* 7(3): 2320–2325. DOI:10.1021/nn305510u. URL <https://doi.org/10.1021/nn305510u>.

Zaburdaev V, Denisov S and Klafter J (2015) Lévy walks. *Rev. Mod. Phys.* 87: 483–530. DOI:10.1103/RevModPhys.87.483. URL <http://link.aps.org/doi/10.1103/RevModPhys.87.483>.